

Fabrication of uranium oxycarbide kernels and compacts for HTR fuel

Jeffrey A. Phillips^{a,*}, Scott G. Nagley^b, Eric L. Shaber^{a,1}

^a Idaho National Laboratory, 1955 Fremont Avenue, Idaho Falls, ID 83415-3855, USA

^b Babcock and Wilcox Nuclear Operations Group, P.O. Box 785, Lynchburg, VA 24505-0785, USA

ARTICLE INFO

Article history:

Received 2 February 2011

Received in revised form

17 September 2011

Accepted 17 September 2011

ABSTRACT

As part of the program to demonstrate tristructural isotropic (TRISO)-coated fuel for the Next Generation Nuclear Plant (NGNP), Advanced Gas Reactor (AGR) fuel is being irradiation tested in the Advanced Test Reactor (ATR) at Idaho National Laboratory (INL). This testing has led to improved kernel fabrication techniques, the formation of TRISO fuel particles, and upgrades to the overcoating, compaction and heat treatment processes. Combined, these improvements provide a fuel manufacturing process that meets the stringent requirements associated with testing in the AGR experimentation program. Researchers at INL are working in conjunction with a team from Babcock and Wilcox (B&W) and Oak Ridge National Laboratory (ORNL) to (a) improve the quality of uranium oxycarbide (UCO) fuel kernels, (b) deposit TRISO layers to produce a fuel that meets or exceeds the standard developed by German researchers in the 1980s, and (c) develop a process to overcoat TRISO particles with the same matrix material, but apply it with water using equipment previously and successfully employed in the pharmaceutical industry. A primary goal of this work is to simplify the process, making it more robust and repeatable while relying less on operator technique than prior overcoating efforts. A secondary goal is to improve first-pass yields to greater than 95% through the use of established technology and equipment.

In the first test, called "AGR-1," graphite compacts containing approximately 300,000 coated particles were irradiated from December 2006 to November 2009. The AGR-1 fuel was designed to closely replicate many of the properties of German TRISO-coated particles thought to be important for good fuel performance. No release of gaseous fission product, indicative of particle coating failure, was detected in the nearly 3-year irradiation to a peak burn up of 19.6% at a time-average temperature of 1038–1121 °C.

Before fabricating AGR-2 fuel, each fabrication process was improved and changed. Changes to the kernel fabrication process included replacing the carbon-black powder feed with a surface-modified carbon slurry and shortening the sintering schedule. AGR-2 TRISO particles were produced in a 6-inch diameter coater using a charge size about 21-times that of the 2-inch diameter coater used to coat AGR-1 particles. The compacting process was changed to increase matrix density and throughput by increasing the temperature and pressure of pressing and using a different type of press. AGR-2 fuel began irradiation in the ATR in late spring 2010.

The high quality UCO kernels used in the AGR fuel tests at ATR were produced by B&W. Fuel for the AGR-1 test (350 μm, 19.7% ²³⁵U-enriched UCO kernels) was produced in 2005. Fuel for the AGR-2 test (425-μm, 14% enriched UCO kernels and 500-μm, 9.6% enriched UO₂ kernels) was produced in 2008. Fuel of the same size and enrichment as AGR-1 kernels were produced for the AGR-3/4 experiment, yet to be irradiated. B&W has also produced more than 100 kg of natural uranium UCO kernels, which are being used in coating development tests. Successive kernel lots also demonstrate consistent high quality and allow for fabrication process improvements. Improvements in kernel forming were made subsequent to AGR-1 kernel production. Following fabrication of AGR-2 kernels, incremental increases in sintering furnace charge size have been demonstrated. Recently, small-scale sintering tests using a small development furnace equipped with a residual gas analyzer (RGA) have increased understanding of how kernel sintering parameters affect sintered kernel properties. The steps taken to increase throughput and process knowledge have reduced kernel production costs. Other modifications have been studied to increase the current fabrication line capacity for producing first core fuel for the NGNP and to provide a basis for the design of a full-scale fuel fabrication facility.

* Corresponding author. Tel.: +1 208 526 0925/8145.

E-mail addresses: jeffrey.phillips@inl.gov (J.A. Phillips), sgnagley@babcock.com (S.G. Nagley), eric.shaber@inl.gov (E.L. Shaber).

¹ Tel.: +1 434 522 5081.

INL and B&W are evaluating an alternative hot-press compaction methodology to yield higher matrix densities, generate less waste, and increase compaction rates without any compromise in compact quality. A variety of process approaches are available and have been historically used to manufacture cylindrical fuel compacts. Jet milling, fluid-bed overcoating, and hot-press compacting approaches being adopted by the U.S. Advanced Gas Reactor Fuel Development Program for scale-up of the compacting process involve significant paradigm shifts from historical approaches. These new methods are being pursued simply to increase yields and eliminate process mixed waste. Recent advances in jet-milling technology simplify dry matrix powder preparation. The matrix preparation method is well matched with patented fluid-bed powder overcoating technology, recently developed for the pharmaceutical industry and directly usable for overcoating high-density fuel-particle-matrix. High-density overcoating places fuel particles as close as possible to their final position in the compact and is matched with hot-press compacting, which fully fluidizes matrix resin to achieve die fill at low compacting pressures and without matrix end caps. Overall, the revised methodology provides a simpler process that should provide very high yields, improve homogeneity, further reduce defect fractions, eliminate intermediate grading and quality control steps, and allow further increases in fuel packing fractions. The compacting process for AGR fuel is being scaled-up from a laboratory process to an engineering-scale process ready for replication to meet production requirements. The scale-up effort was started after a year of planning and evaluation. It continues today on the baseline premise of designing a safe, efficient, and cost effective compacting system and adjusting graphite and resin material characteristics as needed to achieve all specification requirements, high yields, and an optimum product within that design. At this writing, the scale-up effort is 20 months into the execution phase. The B&W compacting facility was readied, and the required scale-up process equipment purchased, factory tested, and received. Its installation is nearing completion. By the end of March 2011, overcoating of natural uranium oxycarbide (NUCO) particles for process finalization testing can begin. The fuel qualification test of AGR-5/6 compacts is scheduled in approximately 23 months, so finalizing the process is gaining urgency. Process engineering work on unit operations for compacting has streamlined the fabrication approach, eliminated waste management issues, and allowed specification, design, and purchase of engineering-scale equipment appropriate for efficient compact manufacturing. A set of process-detail surrogate tests were initiated in the summer of 2010 to determine the components and process parameters appropriate for production compacting.

© 2011 Published by Elsevier B.V.

1. Introduction

The goals of the NGNP/AGR Fuel Development and Qualification Program include providing fuel qualification data to support licensing of the NGNP and supporting near-term deployment of the NGNP in the United States by reducing market entry risks posed by technical uncertainties associated with fuel production and qualification (Petti et al., 2008). Fuel qualification data are being generated by a series of irradiation tests at Idaho National Laboratory (INL). Fuel kernels for all the tests have been or will be produced by Babcock and Wilcox (B&W). As fabrication proceeds from one fuel to the next, processes are being improved to establish a commercially viable fuel manufacturing process.

Uranium dioxide (UO_2) and uranium oxycarbide ($\text{UO}_2\text{--UC}_2\text{--UC}$, often designated UCO) microspheres for high temperature gas-cooled reactor (HTGR) fuel have been fabricated using external gelation, internal gelation, and a combination of these two processes (Vaidya, 2008; Beatty et al., 1979; Charollais et al., 2004; Hunt et al., 2007; Fu et al., 2004; Mehner et al., 1990; International Atomic Energy Agency, 1997). The terms internal and external gelation refer to the source of the ammonia ion that provides a necessary component in the gelation process. In external gelation, the ammonia ion is provided from an external source, such as an ammonia hydroxide vapor, through which the formed particle passes. Internal gelation uses an internal source of ammonia that is normally triggered to release its ammonia by a combination of pH difference and temperature. Kernel fabrication processes include steps of preparing a uranium solution, forming gelled microspheres, sintering the microspheres, upgrading kernels by removing undersized, oversized, and high-aspect-ratio kernels, and performing quality control analyses to verify conformance with fuel specifications.

B&W chose the internal gelation particle process in the late 1980s after reviewing available literature data and consulting with Oak Ridge National Laboratory (ORNL) personnel. B&W has used the internal gelation process to produce various types of particles,

including UC/ UC_2 /UC-ZrC, UO_2 , UCO, and uranium nitride (UN). In the latter case, B&W produced high purity UN for the fabrication of UN pellets using the internal gelation process. The UN particles produced were high-purity and low-density material that could be added directly to the die cavity and pressed to form high-density uniform pellets.

B&W has produced ^{235}U enriched UCO and UO_2 kernels in support of the Advanced Gas Reactor (AGR) tests at INL. Kernels containing natural uranium have also been produced for use in coating tests. Four lots of enriched kernels, three of UCO and one of UO_2 , have been produced along with more than 100 kg of natural uranium kernels.

Two process improvement areas are overcoating and compacting of tristructural isotropic (TRISO) fuel particles into fuel compacts. The traditional approach used to apply the graphite overcoat is to mix synthetic graphite, natural graphite, and phenolic resin and coat the TRISO particles using this mixture and an alcohol (e.g., methanol, isopropanol). Because of the use of alcohols and radioactive components, any waste generated during handling or clean up is automatically classified as a mixed waste, which under US regulations requires a treatment permit to manage. A team of INL, B&W, and ORNL researchers are working to develop a process to overcoat TRISO particles using this same matrix material, applied with water using equipment previously and successfully employed in the pharmaceutical industry. One of the primary goals of this work is to simplify the process, making it more robust and repeatable while relying less on operator technique than prior overcoating efforts. Another goal is to improve first-pass yields to greater than 95% through the use of established technology and equipment.

2. AGR-1 fuel kernels

Irradiation of AGR-1 fuel was very successful, with no particle failures detected over the 3-year irradiation to a burnup of 19% (Grover et al., 2010). Nevertheless, based on the experience

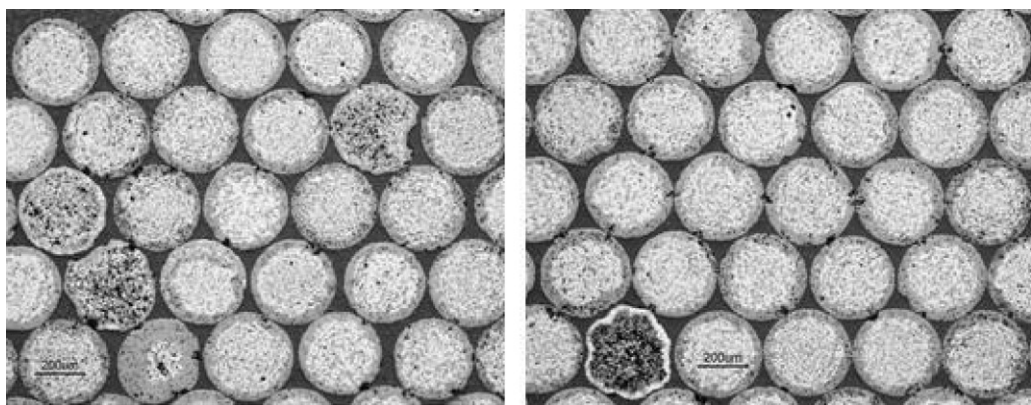


Fig. 1. Images of ceramographic mount kernels from AGR-1 lot.

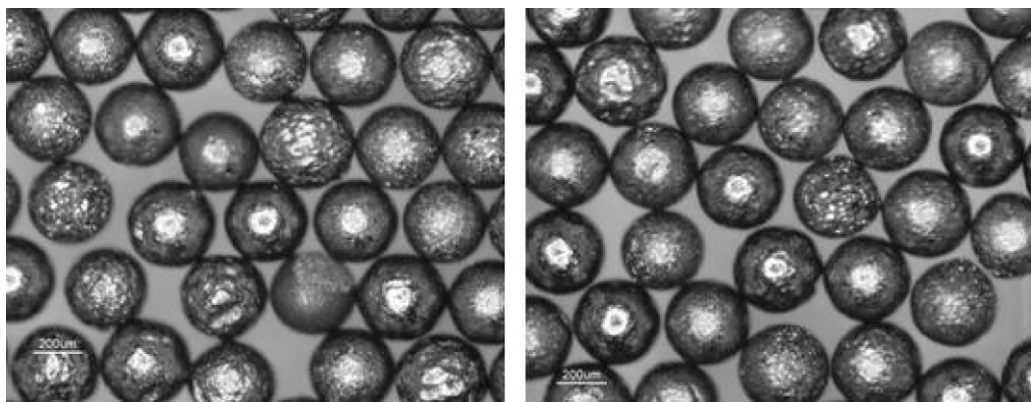


Fig. 2. Images of loose kernels from AGR-1 lot.

of fabricating and characterizing AGR-1 kernels, it was recognized that improvements could be made in kernel product quality and the kernel fabrication process. Kernels from the AGR-1 lot are shown in Figs. 1 and 2. Even though many of the kernels have a similar appearance, differences in chemistry, shape, density, and surface morphology can be seen.

3. Initial process improvement and AGR-3 and 4 kernels

Following production of kernels for AGR-1, B&W performed process improvement tests to reduce the variability of kernel properties within batches and from batch to batch. These tests included evaluating and changing the carbon feed material, changing the

way carbon was mixed into the broth, optimizing broth parameters, and testing alternative sintering schedules. More details and results of these studies were reported at the high-temperature reactor (HTR) 2006 conference (Barnes et al., 2008a).

Kernels for AGR-3 and 4 irradiation tests were produced midway through the process improvement studies, and were produced to the same specifications as AGR-1 fuel. Improvement in quality is visible in the images of the kernels, as is evident in Fig. 3. The sectioned kernels appear much more homogeneous in chemistry and density, and fewer kernels are seen with non-spherical shapes than AGR-1 kernels. Loose kernels appear similar to AGR-1 kernels, except without their showing any highly crystallized surface.

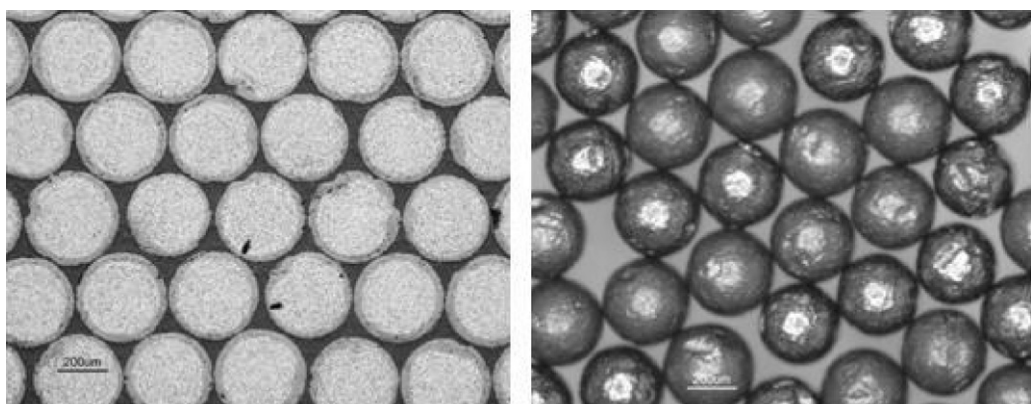


Fig. 3. Images of mounted and loose kernels used for AGR-3 and 4 fuel.

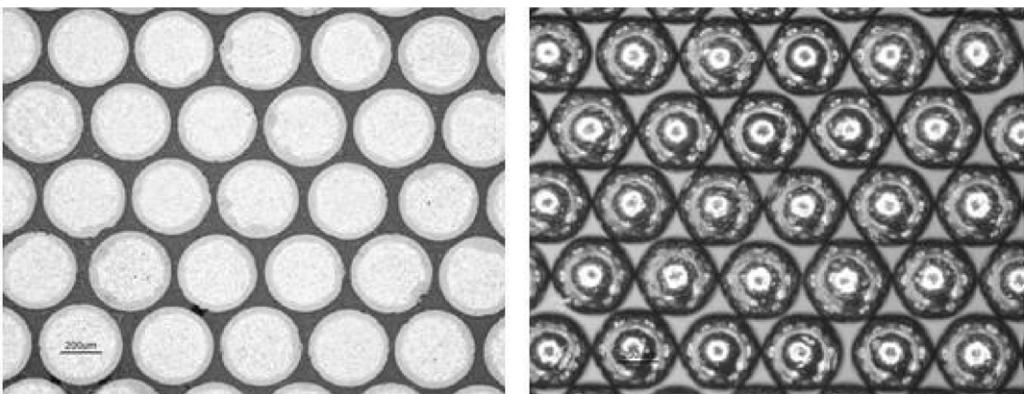


Fig. 4. Images of mounted and loose kernels used for AGR-2 UCO fuel.

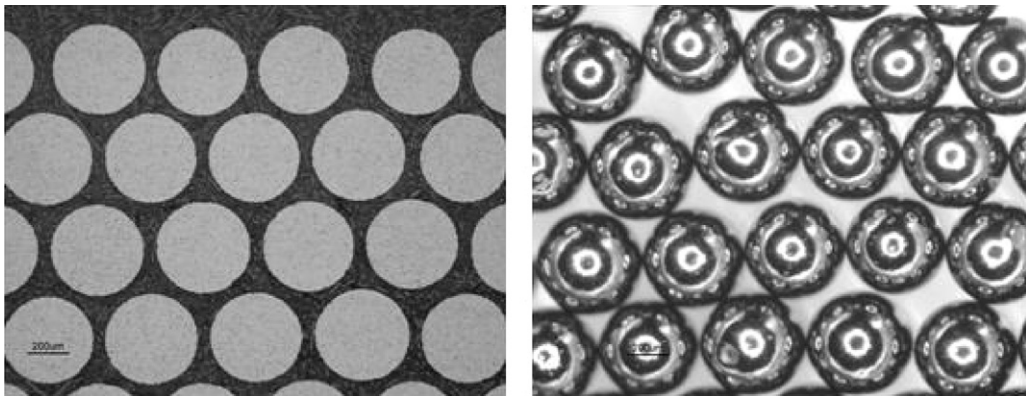


Fig. 5. Images of mounted and loose kernels used for AGR-2 UO₂ fuel.

4. AGR-2 and natural uranium kernels

Kernels for AGR-2 fuel were produced in 2008. The AGR-2 specification for UCO kernels increased the mean diameter from 350 μm (used for AGR-1 and AGR-3 and 4) to 425 μm. The UO₂-kernel mean diameter specification was 500 μm. Five batches of UCO kernels were composited to make up an 8.4 kg lot of 14% enriched UCO product and seven batches of UO₂ kernels composited into an 8.5 kg lot of UO₂ kernels. Images of AGR-2 UCO kernels are shown in Fig. 4 and of UO₂ kernels, in Fig. 5. The most noticeable difference in AGR-2 kernels compared to AGR-1 and AGR-3 and 4 is the appearance of the loose kernels, showing a very smooth, reflective surface.

Six lots of natural uranium kernels were produced from 2007 to 2009, totaling approximately 100 kg. Images from the most recent

lot shown in Fig. 6 have a nearly identical appearance to AGR-2 kernels. This lot of nearly 40 kg included combined kernels from 14 sintering runs plus 6 kg of residual kernels from the previous lot.

5. Property comparisons

AGR requirements for kernels include specifications for diameter, aspect ratio, density, and chemistry. A summary comparison of kernel lot properties is shown in Table 1. The AGR fuel specification document allows a tolerance of ±10 μm on the mean kernel diameter, and Table 1 shows that a deviation of less than 9 μm has always been achieved. The diameter standard deviation is typically 8–12 μm for a kernel lot and 5–9 μm for a kernel batch.

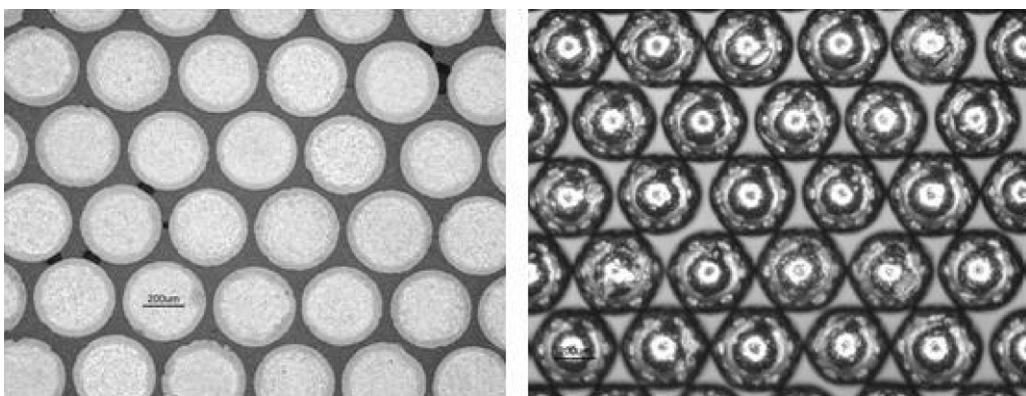


Fig. 6. Images of mounted and loose natural uranium UCO kernels, lot 69311.

Table 1
Comparison of kernel lot properties.

	Mean diameter (μm)	Target diameter (μm)	Diameter standard deviation (μm)	Mean aspect ratio	Aspect ratio standard deviation
AGR-1	348.4	350 ± 10	8.3	1.013	0.016
AGR-3 and 4	358.6	350 ± 10	8.8	1.010	0.012
AGR-2 UCO	426.7	425 ± 10	8.8	1.012	0.007
AGR-2 UO_2	507.7	500 ± 10	11.9	1.008	0.005
Lot 69311	429.3	425 ± 10	11.0	1.011	0.005
	Mean density (g/cm^3)	Density standard deviation (g/cm^3)	Chemistry (mole %)		
AGR-1	10.7	0.026	67.9	0.4	31.7
AGR-3 and 4	10.9	0.030	71.4	8.9	19.7
AGR-2 UCO	11.0	0.030	71.4	12.3	16.4
AGR-2 UO_2	10.9	0.029	100	NA	NA
Lot 69311	10.8	0.023	72.3	13.8	13.9

Table 2
Comparison of kernel properties for “baseline” tests in the two different furnaces.

Run	Mean diameter (μm)	Mean sphericity ratio	Density (g/cm^3)	U	C	C/U	O	O/U	S (ppm)
2.5-inch furnace tests									
59100	423.16	1.012	10.93	89.58	1.80	0.399	8.630	1.433	538
59101	424.60	1.013	10.89	89.54	1.82	0.403	8.625	1.433	580
59103	421.22	1.012	10.85	89.51	1.83	0.404	8.625	1.433	538
6-inch furnace tests									
59426	431.07	1.013	10.55	89.48	1.86	0.411	8.640	1.436	494
59427	423.32	1.011	10.82	89.59	1.86	0.411	8.620	1.431	598

The mean kernel aspect ratio for all lots has been approximately 1.01. This indicates that the kernels formed by the B&W internal gelation process are, on average, more spherical than those formed by other gelation processes, which typically have a mean aspect ratio of 1.05. For example, the mean aspect ratio of German reference fuel kernels, based on analysis of about 6700 kernels from the EUO 2358–2365 composite, was 1.05 (Hunn, 2004). Also, Chinese researchers report an average aspect ratio of 1.04 for 52 batches of kernels using the Total Gelation Process of Uranium (TGU) (Fu et al., 2004). Although aspect ratios of 1.01 are not required to make adequate TRISO particles, the ratio provides a good indicator of the overall kernel quality and process control of the B&W process.

The improvement of product quality over time is clearly seen in the trend of aspect ratio standard deviation. As shown in Table 1, the standard deviation of the aspect ratio for AGR-1 kernels was 0.016, and decreased to 0.012 for AGR-3 and 4 kernels, 0.007 for AGR-2 UCO kernels, and 0.005 for kernels produced after AGR-2 UCO. Mean kernel densities and density standard deviations are very consistent and well above the specification minimum density for all kernel lots.

AGR kernel chemistry specifications include a minimum uranium concentration and specified carbon and oxygen contents,

expressed as mole fractions of carbon/uranium and oxygen/uranium ratios. UCO chemistry is complex, and compositions shown in Table 1 assume the kernels consist entirely of the three compounds UO_2 , $\text{UC}_{1.86}$, and UC . Almost all carbon in AGR-1 kernels was contained as UC , with only a small fraction as $\text{UC}_{1.86}$. The fraction of $\text{UC}_{1.86}$ increased to approximately 9% for AGR-3 and 4 and increased further to 12% for AGR-2 UCO kernels. One means of increasing the kernel carbide content is to change the feed carbon-black-to-uranium ratio in the forming process. A second way is to change sintering conditions.

6. Sintering studies

To support kernel sintering improvements, B&W recently procured and installed a 2.5-inch diameter furnace. A series of 16 tests were performed in this furnace in late 2009 and early 2010 in which process parameters were systematically varied.

The first goal of these tests was to establish that comparable sintered product was produced in the two furnaces when using nominally the same process conditions. The comparison of properties shown in Table 2 and images of kernels shown in Fig. 7 provide confidence that results of the two furnaces were very similar. Based

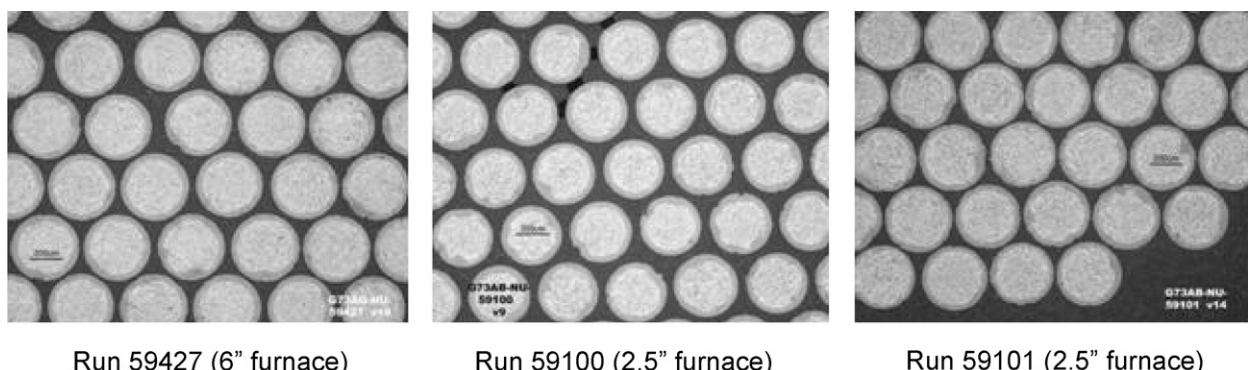


Fig. 7. Comparison of kernels from tests in the two furnaces.

Table 3

Baseline sintering schedule for UCO kernels at B&W.

Segment	Temperature	Process gases	Hold/ramp
1	RT–100 °C	100% Ar	4 °C per min
2	100–550 °C	6% H ₂ and 94% Ar	4 °C per min
3	550 °C	6% H ₂ and 94% Ar	60 min–hold
4	550–1680 °C	100% Ar	40 °C per min
5	1680 °C	100% Ar	4 min–hold
6	1680 °C	60% CO/40% Ar	60 min hold
7	1680–1920 °C	60% CO/40% Ar	40 °C per min
8	1920 °C	60% CO/40% Ar	60 min–hold
9	Cool down	100% Ar	75 °C per min (unregulated)

on results of many other 6-inch furnace runs, the density of kernels from run 59,426 was somewhat anomalous, as densities in the range 10.8–11.0 g/cm³ are nearly always observed.

The sintering schedule used for the baseline tests is shown in Table 3. In one series of tests, the hold time at 550 °C was reduced from the baseline 60 min to 45 min in one test and to 30 min in another. No significant changes in sintered kernel properties were observed.

Decreasing the hold time at 1680 °C without changing the baseline gas composition resulted in slightly lower density (decreasing only from 10.89 to 10.81 g/cm³ when changing from a 60-min to a 4-min hold), no change in UO₂ content, a slight increase in UC₂, a corresponding decrease in UC content, and an increase in the sulfur concentration.

Changing the conditions of the final densification step had the largest effect on both kernel density and kernel stoichiometry. Reducing the temperature from 1920 to 1880 °C resulted in a decrease in density from 10.89 to 10.72 g/cm³, a 24% increase in the UC₂ content, and a slight increase in the UO₂ content. Reducing the sintering time to 30 min without changing temperature reduced the density to 10.58 g/cm³ without significantly affecting kernel chemistry. Changing the gas composition for the densification step from 60% CO/40% Ar to 100% CO resulted in changes similar to reducing the temperature.

Two runs were made at the end of the test sequence in which the most promising changes were implemented into a modified sintering schedule. The changes from those shown in Table 3 were reducing the hold time at 550 °C from 60 to 30 min, reducing the hold time at 1680 °C in CO from 60 to 4 min, and increasing the CO concentration from 60% CO to 100% CO for segments 6 through 8.

These changes were recommended to improve the chemical composition (increasing the UC₂ content) of the UCO kernel product and to improve the sintering cycle efficiency relative to cost and time. The cycle time was reduced by 90 minutes (12% of the total cycle time) and the total CO usage reduced by approximately 20%.

The results of the two runs using the recommended modified conditions are shown in Table 4. They confirm that the desired chemical composition change and production efficiency goals can be achieved. Compared to kernels produced using the baseline sintering schedule, the revised sintering schedule results in a lower density, a consequence of the shift to an increased UC₂ fraction.

Table 4

Results of modified sintering schedule tests.

Run	Mean diameter (μm)	Mean sphericity ratio	Density (g/cm ³)	U	C	C/U	O	O/U	S (ppm)
2.5-inch furnace using baseline tests									
59100	423.16	1.012	10.93	89.58	1.80	0.399	8.630	1.433	538
59101	424.60	1.013	10.89	89.54	1.82	0.403	8.625	1.433	580
59103	421.22	1.012	10.85	89.51	1.83	0.404	8.625	1.433	538
2.5-inch furnace using modified sintering schedule runs									
59115	430.30	1.023	10.55	89.30	1.93	0.430	8.710	1.450	429
59116	427.60	1.013	10.59	89.23	1.89	0.420	8.790	1.470	279

Table 5

Yields from the B&W fabrication process.

	Process yield for (%)			
	AGR-1 UCO	AGR-2 UO ₂	AGR-2 UCO	2009 Natural uranium UCO
Forming	86.2	93.1	93.6	–
Sintering	72.6	77.4	86.6	87.5
Combined	62.6	72.1	81.1	82.9

This modified sintering schedule will undergo additional testing in the pilot-scale furnace.

7. Product yields

Table 5 shows the yields of product kernels from both kernel forming and sintering steps. Scrap product from the forming process results from system holdup and system upset conditions, while scrap from sintering includes undersize and oversized kernels separated by size classification and kernels removed by tabling. Over time, product efficiencies have increased for both the forming and sintering processes. While no specific efforts have been made as yet to improve product yields, the increase is seen as a byproduct of other changes to improve homogeneity and, also, of increased operator experience.

8. Process throughput

The production rate of a full-scale fuel manufacturing plant to support an NGNP has not been clearly established. One estimate of the required annual production is 2400 kg (as uranium) of 350-μm UCO kernels.

The current capacity of the B&W pilot kernel-fabrication line is about 120 kg uranium per year based on a single shift per day, 5-day per week, 40 week per year operation. The rate is limited by the forming line, specifically washing and drying the kernels. With relatively minor modifications to the forming line, and assuming the same operating basis, a rate of 240 kg uranium per year is achievable. The current B&W facility is primarily designed as a development facility and is licensed to handle all uranium enrichments (from depleted to fully enriched materials); the ability to process HEU material limits the throughput capacity of the facility. However, the key components in the system are essentially full-scale equipment that could be used in a production facility. For example, the forming system currently used would be used in a continuous rather than batch mode and would have a multiple-nozzle feed. The product collection system would need to be modified for the larger output, but only in the number of available receivers, and not necessarily in the receiver design. The current sintering furnace, if used in a three-shift operation, could produce up to five runs per week and is capable of charge sizes of 5 kg or more if used in an LEU facility with appropriate nuclear criticality-safety controls. This would permit up to 1000 kg uranium per year from one such furnace. The base systems being developed under this program are

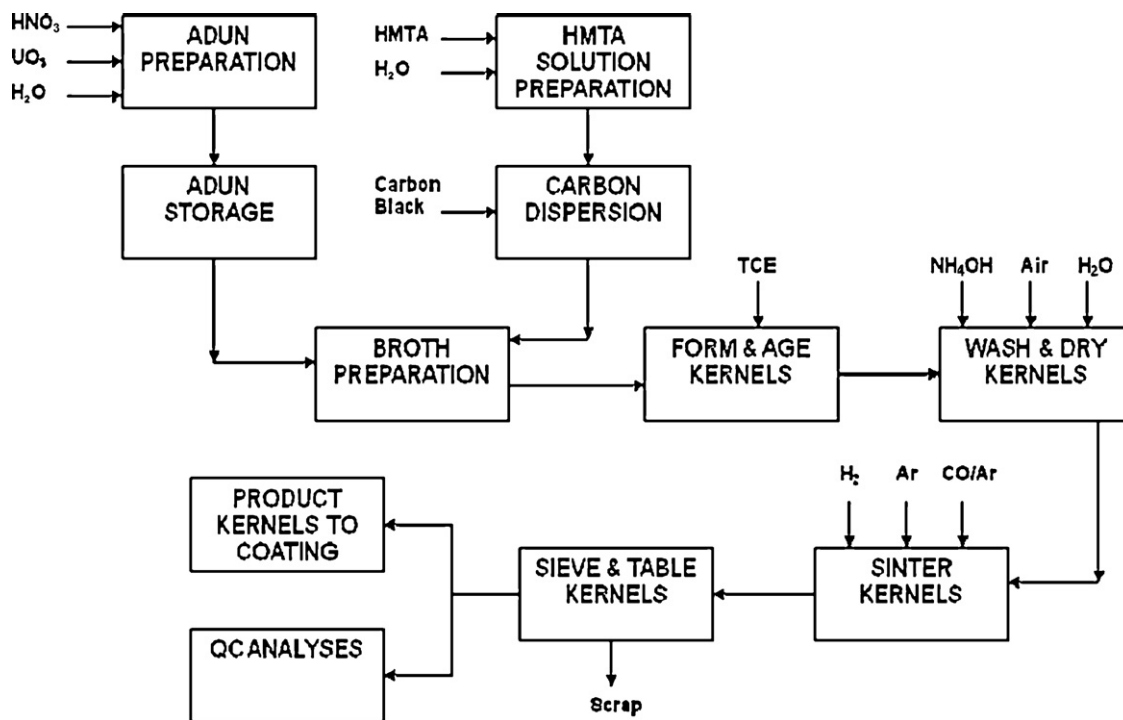


Fig. 8. Schematic showing AGR-2 kernel fabrication process.

readily scalable to a full-size production facility with capacity in ranges sited above.

Both AGR-1 and AGR-2 kernels were fabricated at B&W in pilot-scale equipment using an internal-gelation process. However, minor changes in the process between the AGR-1 and AGR-2 production campaigns resulted in both kernel quality and process improvements (Barnes et al., 2008a, 2010). A block-flow diagram of the process used to fabricate kernels for the AGR-2 experiment is shown in Fig. 8.

8.1. Comparison of kernel properties

Table 6 and Fig. 9 provide comparisons between AGR-1 and AGR-2 kernels. The nominal kernel diameter for the AGR-2 experiment was increased from 350 to 425 μm , and the ^{235}U enrichment was reduced from 19.7% to 14%. The larger kernel size with lower ^{235}U enrichment compared to AGR-1 kernels was based on available NGNP prismatic core design studies for optimizing a single particle/single enrichment system (no fertile particle). Additional advantages of the larger fuel kernel include a reduced packing fraction and easier fabrication.

Table 6
Comparison of AGR-1 and AGR-2 UCO kernels.

Property	AGR-1	AGR-2
Mean diameter, μm	350	427
Diameter standard deviation, μm	8.4	8.8
Mean aspect ratio	1.013	1.012
Aspect ratio standard deviation	0.016	0.007
Ave. enrichment, %	19.7	14
Ave. volume per kernel, cm^3	1.20E-5	4.10E-5
Ave. mass per kernel, mg	0.238	0.445
Ave. mass ^{235}U per kernel, mg	0.042	0.056
Ave. density, g/cm ³	10.6	10.9
Ave. O/U molar ratio	1.36	1.44
Ave. C/U molar ratio	0.325	0.395
Ave. uranium, wt.%	90.1	89.6
Ave. sulfur, ppm	608	365

While both kernel lots meet all AGR fuel specifications, differences are clearly visible. Most noticeable is that the AGR-2 kernels are more uniform in appearance, both internally and externally. The observed uniformity in the polished cross sections is indicative of a more uniform chemistry and density. The uniformity in the external shape and surface morphology also indicates a more uniform internal structure.

As seen in Table 6, both AGR-1 and AGR-2 kernels have very good sphericity, with aspect ratios near 1.01. The greater homogeneity of AGR-2 kernels is seen not only in the smaller aspect ratio standard deviation, but also in the reduction of severe shape defects because of large chips prevalent in more friable kernels (internally porous and externally rough kernels evident in Fig. 2). A reduction in the population of kernels with this gross shape defect results in fewer coated particles with localized high curvature (regions of concentrated stress), which in turn may reduce the risk of particle failure during irradiation.

Another difference in the two kernel lots is their chemistry, as illustrated in Fig. 9. The area defined by the blue rectangle shows the allowable mean oxygen-to-uranium (O/U) and carbon-to-uranium (C/U) ratios for AGR-1 kernels. The AGR-2 kernel specification

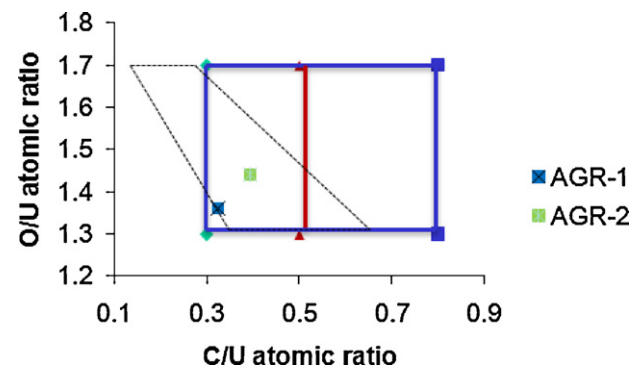


Fig. 9. Comparison of atomic ratios of AGR-1 and AGR 2 kernels.

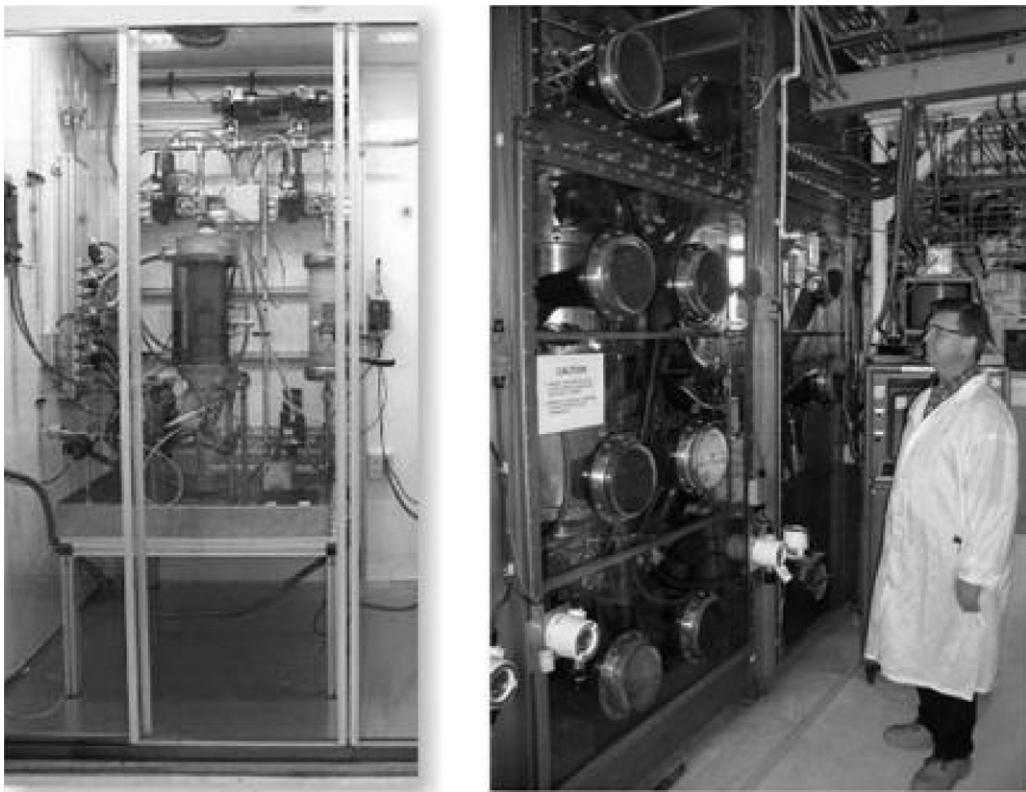


Fig. 10. Coaters used for AGR-1 (ORNL-left) and AGR-2 (B&W-right) particles.

reduced the maximum C/U ratio to 0.5, shown by the red line in Fig. 9. The actual composition of AGR-1 kernels is shown by the blue data point in Fig. 9 and is very near both the specification minimum O/U ratio and minimum C/U ratio. Both ratios were increased in AGR-2 kernels, shown in Fig. 9 by the green data point, so that the target composition was better centered in the composition window, and any subtle changes in composition would still provide kernels that satisfied the composition specification.

The two dashed lines in Fig. 9 shows compositions in which the uranium carbide is present either as 100% UC (left line) or 100% $\text{UC}_{1.86}$ (right line), with the oxygen present as UO_2 . The AGR-1 kernel composition was nearly on the UC line, indicating that its composition was $\text{UO}_2\text{-UC}$, with only a trace of $\text{UC}_{1.86}$. In contrast, AGR-2 kernels had an average composition of 12.3 mol% $\text{UC}_{1.86}$ –16.4 mol% UC–71.4% UO_2 . Increasing the fraction of carbide present as $\text{UC}_{1.86}$ is desirable because it results in a more stable kernel. Carbide present as UC converts to $\text{UC}_{1.86}$ at elevated temperature during coating, with the excess uranium diffusing to the kernel surface to react with the buffer carbon and forming additional $\text{UC}_{1.86}$.

9. Triso-coated particles

AGR-1 kernels were coated in a 2-inch diameter coater at ORNL in batches of approximately 62 g. AGR-2 UCO kernels were coated in a 6-inch diameter coater at B&W facilities in 1300-g batches. Photos of the two coaters are shown in Fig. 10. The coating process has been described in various previous reports and papers (Lowden, 2006; Keeley and Tomlin, 2008; Barnes et al., 2008b). The AGR-1 fuel included a baseline fuel plus three variants produced with different conditions for either the IPyC or SiC layer. One set of coating conditions was used for AGR-2 UCO particles.

Because particle coatings are designed to contain the fission products generated during fuel irradiation, the coating properties

are critical in determining fuel performance. To evaluate the quality of AGR-2 coated particles, comparisons will be made not only of AGR-2 particles to AGR-1 fuel, but also to other historical and international fuels. The comparison between AGR-1 and AGR-2 coated particles is also of interest as it shows the effects of a change in scale of the coating process on the particle properties.

9.1. Thickness standard deviation

One common method of comparing the deposition control of different coaters or coater designs is to compare layer-thickness standard deviations. Low-thickness standard deviations are an indication of even fluidization in a coater, i.e., all particles having nearly the same residence time in regions of the coater with varied coating rate. A comparison of the coating thickness standard deviations for all four coating layers and six fuels are given in Fig. 11.

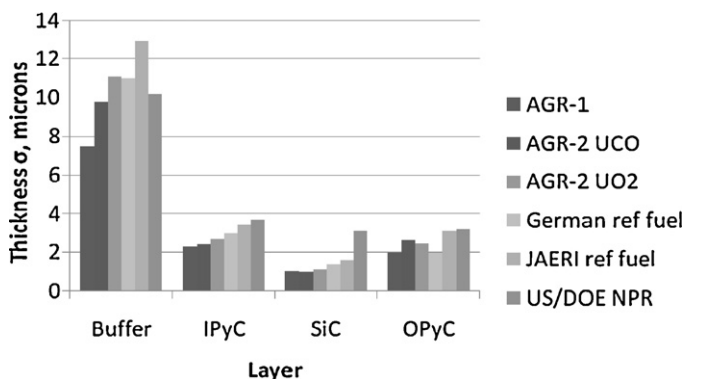


Fig. 11. Comparison of layer thickness standard deviations.

Table 7

AGR-1 and AGR-2 specifications for the maximum allowable particle defect fractions calculated at a 95% confidence level.

Defect	AGR-1	AGR-2
Defects measured before compacting		
Missing OPyC	$\leq 3.0E-4$	$\leq 3.0E-4$
SiC inclusions or “gold spots”	$\leq 1.0E-3$	Info only
SiC burn-leach defects	$\leq 1.0E-4$	$\leq 1.0E-4$
Defects measured after compacting		
Defect	AGR-1	AGR-2
Missing OPyC	$\leq 1.0E-2$	$\leq 1.0E-2$
Defective IPyC	$\leq 2.0E-4$	$\leq 1.0E-4$
Exposed kernels	$\leq 1.0E-4$	$\leq 2.0E-5$
SiC burn-leach defects	$\leq 2.0E-4$	$\leq 1.0E-4$

The AGR-1 thickness standard deviations shown in Fig. 11 are averages for all AGR-1 coating runs (several runs each for baseline, Variant 1–3 composites). The AGR-2 UCO data shown in Fig. 11 are averages of four low-enriched uranium (LEU) coating runs plus 11 natural uranium coating runs (runs 93059–93074). The AGR-2 UO_2 data are the average of three coating runs (93084A, 93085B, and 93086A). Data for German particles are from Hunn (Hunn, 2004); data for Japanese Atomic Energy Research Institute (JAERI) reference fuel, which were used in the HRB-22 test, are from Sawa and Minato (Sawa and Minato, 1999); and data for U.S./Department of Energy (DOE) New Production Reactor (NPR) particles are from General Atomics (1991).

The first observation to be made from Fig. 11 is that the thickness standard deviation correlates with coating rate. The highest deviation for all fuels is for the buffer layer, which has the highest coating rate, and the lowest is for the SiC layer, which has the lowest coating rate. Comparatively, AGR-1 particles had the lowest thickness standard deviations for all four coating layers. AGR-2 particles, both UCO and UO_2 , had the next lowest standard deviations for the IPyC and SiC layers and were within the range of the other fuels for the other two layers. For three of the layers, the U.S./DOE NPR fuel showed the highest thickness standard deviations.

9.2. Particle defect fractions

The AGR-1 and AGR-2 fuel specifications included maximum allowable defect fractions for the coated particles before and after compacting. There were three defect specifications for the coated particle composite and four for the compacted particles as shown in Table 7. Some of the specifications for maximum allowable defect fractions for AGR-2 were reduced to reflect the expected quality of the fuel based on AGR-1 experience and to move toward the low defect fractions that will eventually be required for AGR fuels.

Maximum defect fractions were calculated to 95% statistical confidence from the number of defects measured in a random sample of known size using a binomial distribution method. Comparison of defect fractions can sometimes be misleading because of values reported at different or unreported confidence levels or because of significantly different sample sizes. For that reason, the number of measured defects, sample sizes, and measured defect ratios for each sample are also reported below.

Particles were visually inspected for missing or damaged outer pyrolytic carbon (OPyC) layers before and after compacting. After compacting, this required deconsolidation of the compact and removal of the compact's graphite matrix from the OPyC surface (see Section 9.4). Deconsolidation was achieved electrolytically in concentrated nitric acid.

No particles with missing OPyC layers were found in samples of about 31,000 particles from each of the AGR-1 particle composites before compacting. After compacting, one compact from each of the four AGR-1 fuels was electrolytically deconsolidated, but no

missing OPyC was observed. Similarly, no particles with missing OPyC layers were found in AGR-2 UCO particles before or after compacting. Four particles with missing OPyC layers (bare kernels) were found in the AGR-2 UO_2 particles in a sample of 15,800 particles. The AGR-2 UO_2 particles were subjected to additional upgrading by using a roller-micrometer to remove the smaller diameter, uncoated kernels. No particles with missing OPyC layers were found in AGR-2 UO_2 fuel after compacting.

An important requirement for inner pyrolytic carbon (IPyC) layers is that permeability be sufficient to limit intrusion of chlorine during the deposition of the SiC because chlorine can attack the kernel, resulting in uranium dispersion into the surrounding buffer. Particles were determined to have defective IPyC if X-radiography showed excessive uranium in the buffer region compared to a visual standard. IPyC defects were determined after compacting because high-temperature heat treatment of the compacts makes uranium dispersion much more evident.

No IPyC defects were found in any AGR-1 particle batches in samples of about 50,000 particles each. No IPyC defects were found in a sample of 64,500 AGR-2 UCO particles. One particle was identified to have a defective IPyC layer in a sample of 61,700 AGR-2 UO_2 particles. However, particle analysis indicated that the observed uranium dispersion may have been caused by contamination during coating, rather than having a permeable IPyC.

SiC inclusions, also sometimes referred to as “gold spots” or “SiC laminar (or lenticular) flaws,” are circumferential areas of low-density silicon carbide or carbon embedded in the SiC layer or present at the IPyC/SiC interface that may indicate undesirable fluidization patterns in the coater (Minato et al., 1994). SiC inclusions can span a wide range of sizes (as measured by surface area of gold spots or by thickness and angle of circumferential extent of the actual inclusion). Historically, gold spots have been determined by visual analysis of particles after the OPyC layer had been burned off. These gold spots are caused by light passing through the SiC layer and scattering off the inclusion. However, this optical manifestation is not easily distinguished for particles with small-grained SiC microstructures because of optical scatter at the grain boundaries. An alternative method that involves examination of a large number of mounted particles has therefore been used for AGR-2 fuel.

A correlation of SiC inclusions with irradiation performance has been suggested (Scott and Kovacs, 1977), but is not well established. This may be due in part to the difficulty in defining the point at which a SiC flaw should be counted as a defect. The AGR-1 fuel specification included a visual standard to define the size of a gold spot that should be counted as a defect. The AGR-2 fuel specification required only that SiC inclusions be looked for and reported, given that no inclusions were observed in several coating runs during development. Ninety-five percent confidence limits (CL) on gold spot defect fractions for AGR-1 particles ranged from $\leq 2.5E-4$ to $\leq 1.0E-3$. SiC inclusion defect fractions for AGR-2 fuel batches were in this same range. However, in part, this reflects smaller sample sizes used for AGR-2 particle analysis.

Uranium contamination was determined by repeated nitric acid leaching of the fuel particles and matrix material after electrolytic deconsolidation of the compacts. This uranium contamination may come from fuel kernels not contained by the TRISO coatings and/or tramp uranium from other sources. Tramp uranium may come from matrix materials or be introduced during processing and handling. Uranium contamination values much less than the amount of uranium contained within a single kernel can be assumed to be because of tramp uranium alone. AGR-1 and AGR-2 compacts with no exposed kernels showed negligible levels of tramp uranium.

The AGR-1 and AGR-2 specifications included a maximum allowable defect fraction for particles with exposed kernels (Table 7). Because tramp uranium was determined to be negligible, it has been assumed that the uranium contamination determined

Table 8

Comparison of burn leach defect particles before compacting.

Fuel type	Burn-leach defects	Sample size	Ratio	95% Confidence limits
AGR-1 baseline	0	120,688	0	$\leq 2.5\text{E-}5$
AGR-1 Variant 1	1	121,117	8.3E-06	$\leq 4.0\text{E-}5$
AGR-1 Variant 2	1	50,265	2.0E-05	$\leq 9.5\text{E-}5$
AGR-1 Variant 3	1	120,660	8.3E-06	$\leq 4.0\text{E-}5$
AGR-2 UCO	5	217,159	2.3E-05	$\leq 4.8\text{E-}5$
AGR-2 UO ₂	1	120,000	8.3E-06	$\leq 3.9\text{E-}5$
German particles (Nabielek et al., 2004)	102	3,300,000	3.1E-05	$\leq 3.6\text{E-}5$

by the deconsolidation and acid leaching provides a good measure of the exposed kernel defect fraction. The number of exposed kernels was calculated by dividing the measured uranium contamination by the uranium content in a single kernel. As expected, this value was typically close to a whole number.

After completion of the compact deconsolidation and acid leaching, particles and matrix residue were heated to 750 °C in air to oxidize any exposed carbon. This burn was then followed by additional leaches in nitric acid. The number of particles with uranium exposed by this burn-leach process was again calculated by dividing the measured uranium contamination by the uranium content in a single kernel.

This entire process described above is known as leach-burn-leach (LBL). When performed in full, the pre-burn leach will detect particles with completely broken or missing TRISO coatings, and the post-burn leach will detect particles with defective SiC layers, but at least one good pyrocarbon layer. Exposed kernels detected in the pre-burn leach can be expected to readily release fission products at the start of irradiation. Particles with burn-leach defects may contain most fission products until the pyrocarbon layers fail.

For AGR-1 and AGR-2 fuel, as-coated particles were only subjected to a burn-leach analysis; the pre-burn leach step was not performed. For this reason, the burn-leach defects reported for particles before compacting may also include contributions from what has been described above as uranium contamination (exposed kernels). It should be noted that performing full LBL analysis on particles before compacting can be useful in determining the source of defects. This can also help to elucidate whether the exposed kernels detected after compacting were caused by coatings broken during the compacting process or before.

A comparison of burn-leach defects measured on particles before compacting is shown in Table 8. Burn-leach defects in AGR-1 particles were consistently very low. Combining the data for the four particle composites, three defects found in 317,635 particles equates to a simple ratio of 9.4E-06 and a 95% confidence defect fraction of $\leq 2.4\text{E-}5$. Having completed the 3-year, 19.6% burn-up of AGR-1 fuel without any particle failures, this low defect fraction measured for the as-manufactured particles have been verified.

Burn-leach defects in particles produced in the B&W 6-inch coater prior to AGR-2 particle fabrication were not consistent. Some batches showed levels as low as or lower than AGR-1, while burn-leach defects in other batches were higher. The batches selected for use in AGR-2 had defect fractions comparable to AGR-1 and German fuel.

Particles with cracks through all four layers were found to be the primary type of burn-leach defect in AGR-2 particle batches. These cracks were observed to originate from a single impact point on the outer pyrocarbon layer, indicating the defects were produced after coating was completed. An example of a cracked particle is shown in Fig. 12. Since the fabrication of AGR-2 particles, a thorough review of the B&W coating process has been completed

and changes were made in unloading and upgrading equipment to reduce the risk of cracking particles during handling. Burn-leach defects in AGR-1 fuel were observed, in some cases, to originate from porosity in the SiC layer caused by fluidization anomalies (related to the observed gold spot defects). LBL results discussed below, as well as observations on the severity of SiC inclusions, indicate that SiC defects resulting from fluidization anomalies can be expected to be lower for the 6-inch coater. It is postulated that burn-leach defect fractions can ultimately be reduced below the already low levels observed for AGR-1 through improved handling of the particles produced by the larger coater.

Table 4 shows LBL results for particles recovered from electrolytically deconsolidated compacts. No uranium contamination defects were found in AGR-1 compacts, but a total of three SiC defects were found in 195,605 particles. The reverse was true for AGR-2; a few uranium contamination defects, but no SiC defects, were found. The 95% confidence defect fraction limits were within a tight range for all the fuels, in part because of the larger samples analyzed for AGR-2. Likewise, the lower SiC defect 95% confidence limits for AGR-2 fuel compared to AGR-1 reflect, in part, the larger AGR-2 sample sizes.

Venter and Nabielek (2006) have reported the free uranium fraction for German fuels produced at different times, and these values are reproduced in Table 5. Based on a comparison of defect fractions shown in Tables 9 and 10, both AGR-1 and AGR-2 fuels are very similar to German fuel in this aspect.

9.3. SiC microstructure

A comparison of grain size of the SiC layer is shown in Fig. 13. For AGR-1, the baseline, Variants 1 and 2 particles all had a very similar grain size. Coating conditions were varied for Variant 3 to achieve a smaller grain size. The SiC coating conditions and microstructure for AGR-2 particles, both UCO and UO₂, were most similar to those

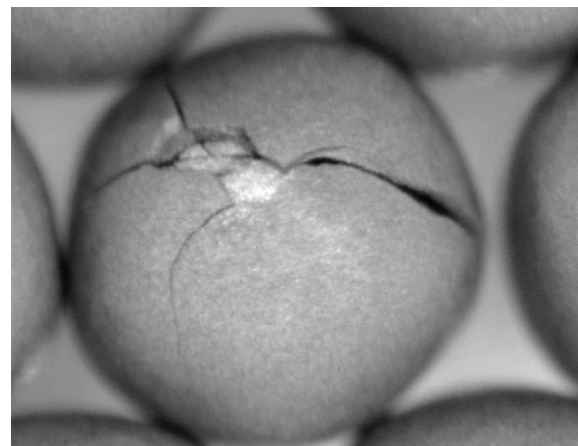


Fig. 12. Cracked particle suspected to be damaged during the unloading process.

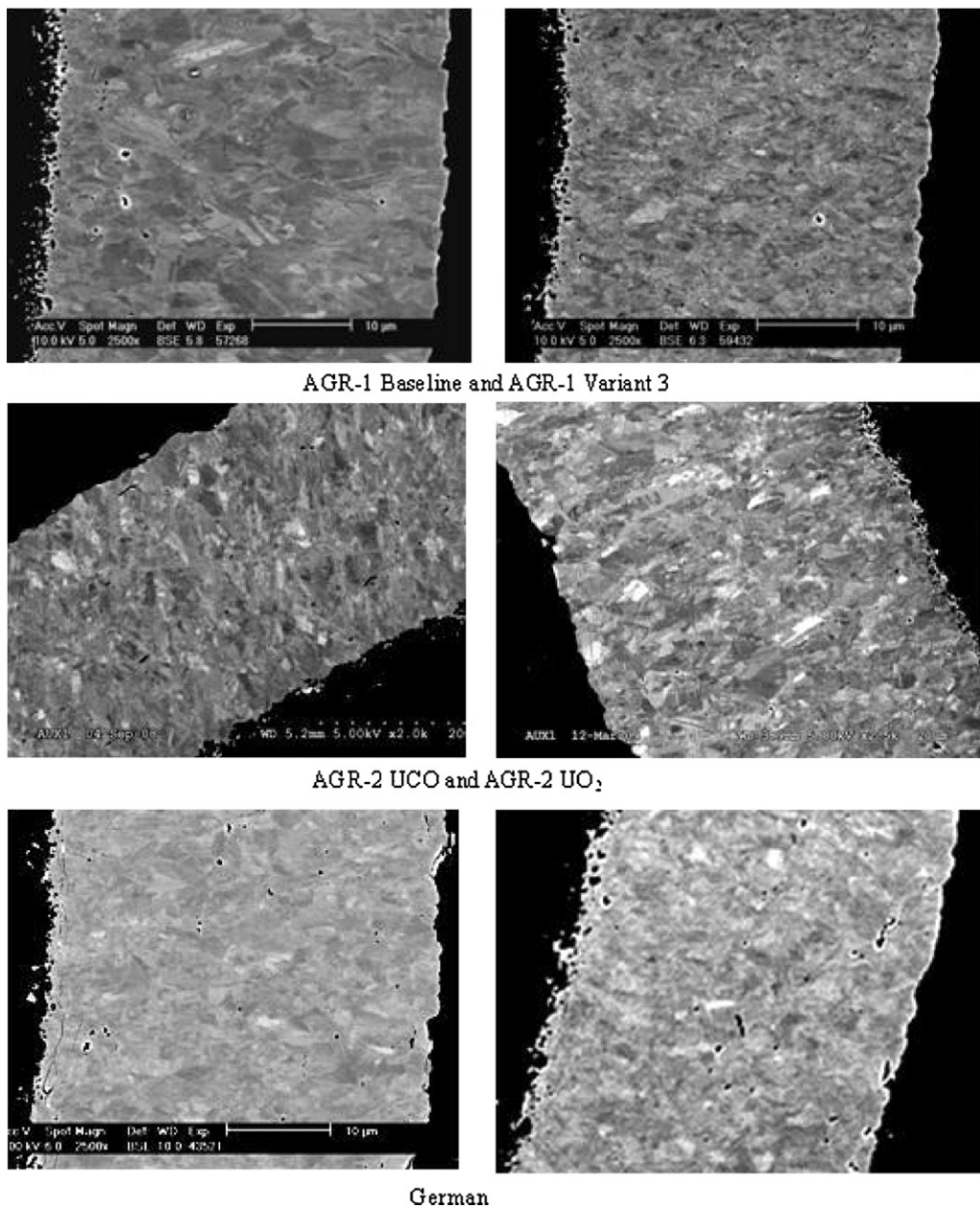


Fig. 13. Comparison of SiC microstructure for AGR-1, AGR-2, and German particles.

Table 9
Comparison of defects found in deconsolidated particles by LBL.

Fuel type	Defects found	Sample size	Ratio	95% Confidence limits
Uranium Contamination (pre-burn leach)				
AGR-1 baseline	0	99,470	0	$\leq 3.1E-5$
AGR-1 Variant 1	0	74,699	0	$\leq 4.1E-5$
AGR-1 Variant 2	0	99,100	0	$\leq 3.1E-5$
AGR-1 Variant 3	0	99,032	0	$\leq 3.1E-5$
AGR-2 UCO	3	317,625	9.4E-06	$\leq 2.5E-5$
AGR-2 UO ₂	3	246,840	1.2E-05	$\leq 3.2E-5$
SiC Defects (post-burn leach)				
AGR-1 baseline	2	49,735	4.0E-05	$\leq 1.3E-4$
AGR-1 Variant 1	0	49,799	0	$\leq 6.1E-5$
AGR-1 Variant 2	1	49,555	2.0E-05	$\leq 9.6E-5$
AGR-1 Variant 3	0	49,516	0	$\leq 6.1E-5$
AGR-2 UCO	0	254,100	0	$\leq 1.2E-5$
AGR-2 UO ₂	0	123,420	0	$\leq 2.5E-5$

of AGR-1 Variant 3. The grain size of AGR-2 particles also closely matches that of German particles.

9.4. Pyrocarbon anisotropy

Comparisons of pyrocarbon anisotropy between different fuel manufacturers can be misleading because of the various methods and instruments used to determine this property. Values shown in Table 11 were all generated by ORNL using the Two-Modulator Generalized Ellipsometry Microscope (2 MGEM) (Jellison et al., 2006; Jellison and Hunn, 2008). In general, AGR-1 particles had a very low anisotropy, and coating conditions for Variant 1 were purposely set to achieve an even lower anisotropy. The anisotropy of the IPyC layer of AGR-2 particles was intermediate between the low anisotropy AGR-1 particles and typical German fuel, while the anisotropy values for the OPyC layer of AGR-2 particles were very close to that of German fuel.

Table 10

Free uranium fraction of German fuels (Venter and Nabielek, 2006).

Fuel designation	GLE 3	LEU Phase 1	GLE 4	GLE 4-2	Proof test
Year of manufacture	1981	1981	1983	1985	1988
Number of particle batches	65	1	54	38	8
Coating batch size, kg	5	5	3	3	5
Free uranium fraction	5.1E-05	3.5E-05	4.3E-05	7.8E-06	1.35E-05

Table 11

Comparison of pyrocarbon anisotropy.

	IPyC layer		OPyC layer	
	Diattenuation	BAFo	Diattenuation	BAFo
AGR-1 baseline	0.0074	1.015	0.0063	1.013
AGR-1 Variant 1	0.0047	1.009	0.0044	1.009
AGR-1 Variant 2	0.0075	1.015	0.0059	1.012
AGR-1 Variant 3	0.0098	1.020	0.0071	1.014
AGR-2 UCO	0.0116	1.023	0.0088	1.018
AGR-2 UO ₂	0.0111	1.022	0.0073	1.015
German reference fuel	0.0140	1.028	0.0080	1.016

10. Overcoating matrix preparation

The carbon/resin-matrix fabrication process combines natural flake graphite, synthetic graphite, a two-part phenolic resin (high purity novolac resin base and hexamethylenetetramine [Hexa]) in such a way that a fully homogenous, inseparable mixture is attained. Historically, matrix preparation was done by solvating the resin in the mixture with ethanol, followed by mixing, drying, and grinding. For AGR scale-up, a volatile organic compound (VOC)-free process is being adapted to minimize process steps, process time, waste generation, and impact to the environment. Moreover, eliminating the use of VOCs eliminates the need for equipment and removes the associated facility from class 1, division 1 electrical requirements requiring explosion-proof motors that are required for use with VOC's (National Electrical Safety Code, 2007).

The process to prepare the carbon/resin matrix mixture is depicted graphically in Fig. 14. Natural graphite, synthetic graphite,

and the two-part novolac phenolic resin are weighed out in nominal ratio of 64%, 16%, and 20% (by weight), respectively. (Hexa is considered part of the resin component, added to achieve desired curing properties.) Gross mixing is performed in a blender prior to final homogenization. The mixture, which is still somewhat separable by mechanical means, is loaded into a volumetric feeder. Jet milling is used to provide final homogenization and size reduction to a nominal 10 μm average particle size with a tight distribution through particle-to-particle high-energy impacts. For development efforts, a 30.5-cm (12-inch; Model 08-626C-SS) orbital jet mill from Jet Pulverizer Company was selected. This equipment uses multiple jets and feed-input locations to maximize particle impacts and milling rates.

Several trials were performed at the Jet Pulverizer Company to test the feasibility of this equipment by mixing natural graphite, synthetic graphite, and phenolic resin in the 64/16/20 ratio identified above. Finished powders as fine as 2.5 μm were produced using this technique. The smallest usable-size powder is ~4.0 μm due to the difficulty of wetting the high surface area of smaller powders.

11. Overcoating process

Overcoating in TRISO fuel fabrication process (1) provides all the matrix required to form the compact, (2) protects the fuel particles from damage during handling and compacting, (3) evenly separates the fuel particles to allow formation of a homogeneous array, and (4) creates a stable phase with good thermal properties (thermal conductivity) for high-temperature use in nuclear applications. While performing these functions, the overcoating must not bond

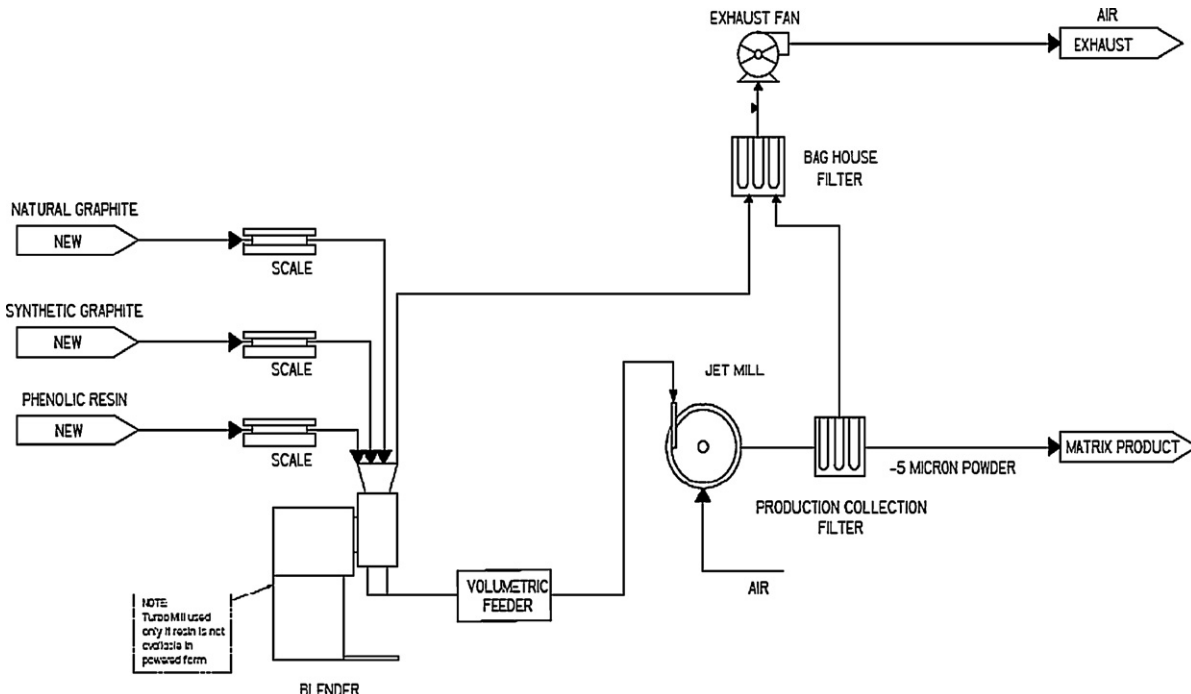


Fig. 14. Schematic showing steps for the graphite/resin matrix.

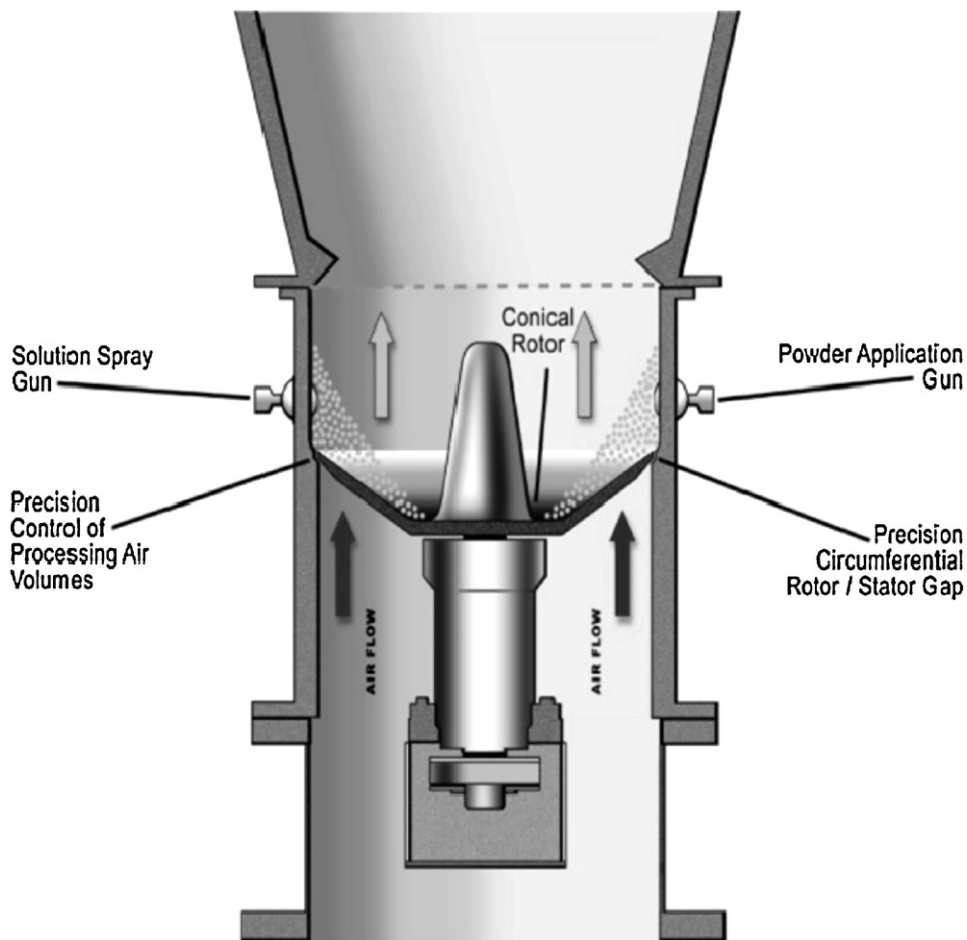


Fig. 15. Cross section showing the Vector overcoating system technology.

excessively to the OPyC layer of the fuel particles because excess adhesion may lead to failure of the OPyC and, thus, to particle failure (Bullock, 1993).

The goal in overcoating is to evenly coat TRISO particles with a consistent thickness of the graphite/resin composite matrix (Petti et al., 2002). This helps reduce the likelihood for damage to the fuel particles from particle-to-particle contact or from damage during compaction (Petti and Bell, 2005; Pappano, 2007). The mass of matrix overcoat applied to the fuel particles is determined by the desired volume packing fraction of the finished compacts for a specific matrix density. Application of 1.19 g of matrix per gram of fuel particles (an approximately 275 μm thick overcoat) to the surface of AGR TRISO particles (Petti et al., 2002) is sufficient to yield a compact with 35% packing fraction. Overcoating has been historically accomplished using drum rolling processes with matrix resin activated with methanol, and testing at ORNL using a modified centrifugal system has proven to be successful for overcoating and compaction for the AGR-1 and AGR-2 fuel tests (Kasten, 1981). Both drum and centrifugal overcoating systems mix a batch of particles and solvated matrix together and work to achieve nominal sphericity by rolling. The scale-up fluid-bed overcoating approach builds layers of matrix powder on the fuel particles using water, keeping the fuel in the center of the highly spherical overcoating and yielding very consistent, highly spherical particles without twins, eccentric particles, or matrix chunks. In the scale-up overcoating process, all matrix components, including Hexa, are applied to the surface of the TRISO particles, but no reaction or curing of the resin takes place as part of overcoating. This is an essential change from historical methods where resins were reacted

before or during overcoating to result in a thermoplastic overcoat product.

Compact packing fractions as high as 35–40% are obtainable with drum-overcoated particles (Pappano, 2007; Kasten, 1981; Morris et al., 2004); drum-process feasibility at higher packing fractions is questionable. Reactor designers have indicated a need for compacts with packing fractions up to 46% or higher. Fluid bed overcoating has demonstrated the feasibility to overcoat particles for 47% packing fraction compacts without the need for any upgrading (sieving or tabling) and no rejects.

The fluid bed overcoating process (Fig. 15) uses the upward movement of air and a rotating chamber to initiate radial and vertical movement and particle spin to the material to be coated. This creates an efficient fluid bed for the overcoating process. While the material is fluidized, the particles are wetted with an atomized liquid (water) sprayed into the bed, and the carbon/resin-matrix powder mixture is vacuum inducted into the chamber. Wetted particles in the fluidized bed pick up the carbon/resin matrix dust mixture on their surface as they spin through the powder cloud. As they lose velocity, they fall back onto the rotating bed, drying and compressing the carbon/resin matrix on their surface. As this process repeats, a uniform layer of carbon/resin matrix builds up on the surface of the particle. Once the proper amount of coating has been applied (as measured by the mass of carbon/resin matrix fed into the overcoater), the feed is suspended, and the coated particles are dried and polished by passing warm ($\sim 80^\circ\text{C}$) air over the wet overcoated particles while being continuously fluidized in the bed. The particle temperature is below room temperature during processing due to water evaporation. When the overcoated particle temperature

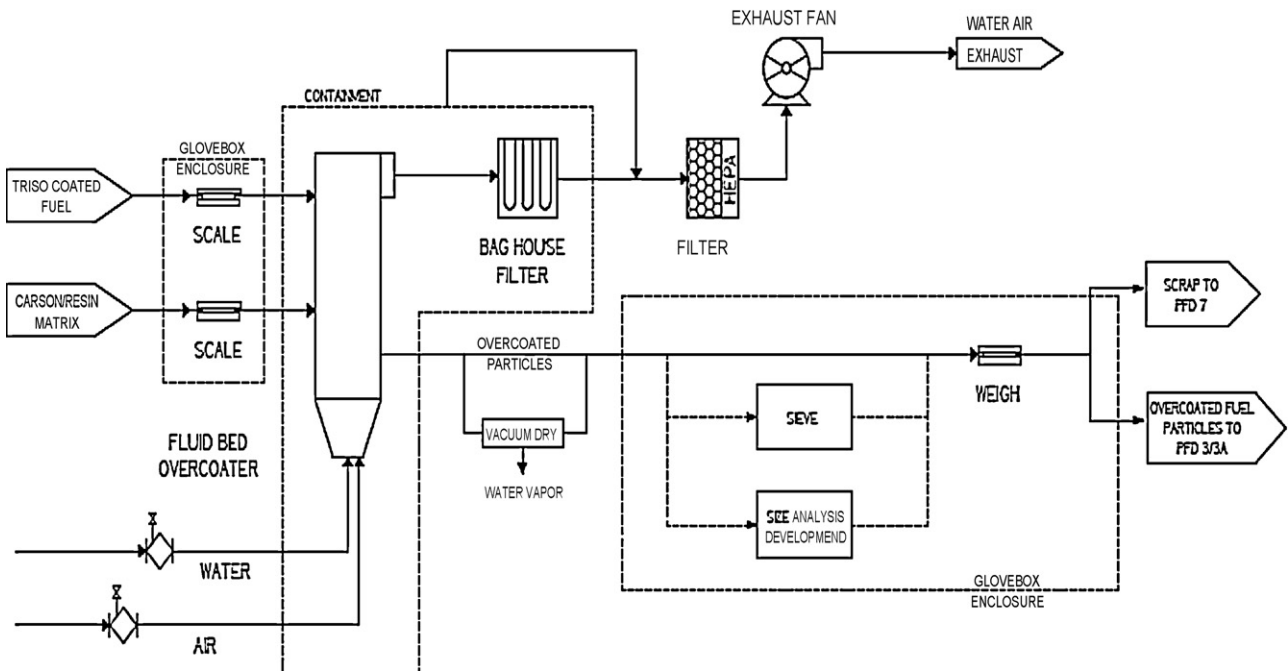


Fig. 16. Schematic of B&W overcoating process.

reaches room temperature, the particles are essentially dry and are removed from the overcoater. The product is then placed in a vacuum dryer for 4 h to ensure that any residual water is removed.

A graphical flow diagram of the pilot plant overcoating process is shown in Fig. 16. TRISO coated fuel particles are weighed in an inert, ventilated enclosure. The fuel charge is loaded into the overcoater (Fig. 17) through the view port from the special double-valved bottle into the mixing chamber to ensure that the particles cannot be spilled. The mixing chamber (Fig. 18) has opposing liquid and matrix feed ports and a thermocouple to measure bed temperature. With this approach, the unit does not need to be opened except for cleaning. The carbon/resin matrix is loaded into the mass flow auger

feeder. Water is measured and placed in a container for metered feed into the overcoater system. The slit air and bed rotational unit are activated, water is fed into the system using the metering pump, and matrix powder is vacuum inducted into the unit to start the overcoating cycle.

12. Compaction

Hot-press compacting places a specific volume of overcoated particles into a die cavity heated above the mettler drop point of the resin and applies force to the die cavity while the resin melts, allowing the matrix to flow around the fuel particles, then begin to



Fig. 17. Photograph of the Vector AGR overcoater on the production floor at B&W.

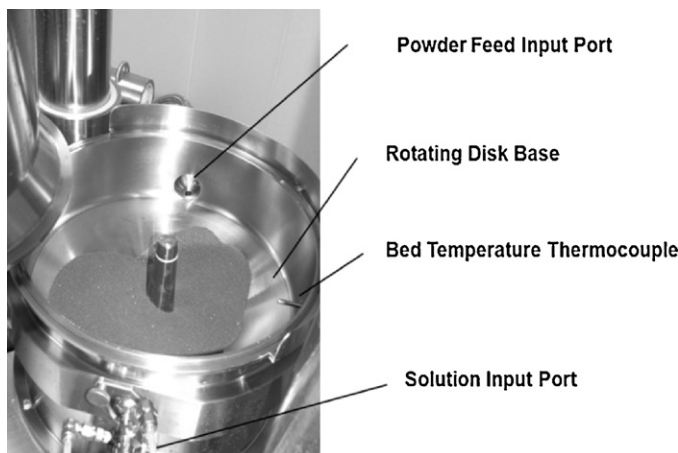


Fig. 18. Vector VLC-lab 3 overcoater base separated from the head to allow loading of surrogate proppant.

set from reaction with formaldehyde generated by decomposition of the Hexa.

The resin and Hexa react during compacting and subsequent thermal treatment (carbonization) to produce a rigid, thermally set material with good thermal conductivity and strength, which protects the fuel particles (Morris et al., 2004). The matrix must not soften or change shape after compacting, so the matrix is partially cured while under pressure in the die cavity. Volatile organics from the resin and Hexa are driven off during carbonization (Charollais et al., 2008). Final vacuum heat treatment then removes most other impurities and improves the thermal conductivity of the final compact. The final heat-treated matrix material must be able to withstand the high temperatures and radiation exposure in a nuclear reactor without undergoing excessive anisotropic dimensional changes or material degradation (Bullock and Sterling, 1977).

Hot-press compaction as described meets the following design requirements:

- Place the desired and repeatable mass of fuel particles into a homogeneous array within the correctly sized compact shape.

This will be accomplished through volume loading of overcoated material.

- Use minimum force to obtain complete die fill and prevent particle breakage while providing a robust compact (high green strength for automated material handling).
- Partially cure resin in the die to ensure particle protection even during tooling ejection while minimizing cycle time
- Provide for high matrix density with minimum internal porosity.
- Provide compacts absent of chips, cracks, or irregularities.
- Provide a process suitable for mass production of fuel compacts in an automated fashion in a suitable compaction press.
- Meet applicable fuel-specification requirements for dimensions, integrity, and density after heat treatment.

The hot-press compaction process will be matched with the flow, thermal characteristics, and set time for the selected resins. This is enhanced through the use of isotherm measurement of resin viscosity as a function of time.

A hot-press compacting system (Fig. 19), built by Miller Tool and Die Co., has been installed and tested at B&W for compact formation. The system makes 4 compacts at a time using an automated volumetric feeder with a single ram operating four punches with nitrogen force-equalizing springs. It also has automated unloading and lubrication and runs in a completely automated manner while making compacts and recording relevant compacting parameters on every compact for record.

Optimization in compacting involves setting the right time, temperature, and pressure to achieve the desired compact properties and matrix density for particles overcoated with matrix for a specific packing fraction. The desired parameters are determined through statistically designed tests that reveal the interrelationship between the compacting variables for a given matrix composition and packing fraction.

13. Thermal treatment

Thermal treatment of fuel compacts has routinely consisted of a carbonization process performed under flowing inert gas and a final heat treatment process performed under vacuum using separate equipment. The scale-up program reviewed these operations and determined that significant improvements could be made



Fig. 19. Miller compaction press at B&W.



Fig. 20. Centorr carbonization/heat treatment furnace at B&W.

by carbonizing the compacts under a partial vacuum to assist in volatile organic removal while retaining a flowing sweep gas to remove the products of volatilization to an external trap. It was also determined that the carbonization and heat treatment portions of the process could be done in the same furnace equipment using updated technology. Overall, these process innovations allow for the carbonization to be followed directly by final heat treatment without any removal or handling of the compacts and without the additional cooldown and heatup involved with historical processes. For the scale-up process line, a Centorr debinding/high temperature vacuum furnace (Fig. 20) was installed at B&W for carbonization and heat treatment of compacts.

14. Results

Overcoating consisted of feasibility tests performed at Vector Corporation lab facilities in Marion, Iowa, using Plenco 14043, Hexion AD5614 and Hexion SD-1708 novolac resin-matrix mixtures. The matrix mixtures were obtained by jet milling natural and synthetic graphites and the resin (containing Hexa) to mean particle sizes from 2.5 to 10 μm (with 2.9 μm standard deviation) at 27 kg/h. Jet milling did not show any visible separation or incomplete milling. Particle size was measured using a Horiba LA950 laser-light-scattering particle-size system at Jet Pulverizer. An alumino-silicate proppant served as surrogate TRISO particles for overcoat testing. The proppant was selected because it had a density ($\sim 3.3 \text{ g/cm}^3$) and size (875–1250 μm diameter) that made it a suitable substitute for TRISO fuel particles even though the sphericity of the proppant was less than desirable. Overcoat feed materials and overcoated particle dimensions were measured using a QICPIC particle-size analyzer at Vector Lab facilities.

Photographs of the overcoated proppant and a cross section of the overcoated particles are shown in Figs. 21 and 22, respectively. The particle-size analysis and the photographs confirmed the ability of the vector overcoat process to apply a relatively uniform and spherical coating on particles that are non-uniform in both size and shape. Overcoating with water proved quite successful and yielded an overcoated particle with average particle size of 1700–2000 μm in diameter (Fig. 23). The curing agent used in the novolac resin, Hexa, acts as a water-soluble binder and provides sufficient green strength to the overcoated particles to allow them to be transported across the United States without damage to

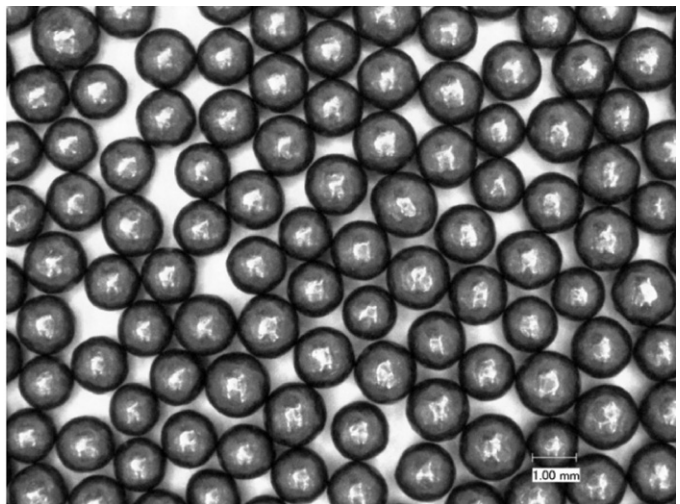


Fig. 21. Photomicrograph of surrogate proppant overcoated with graphite/resin matrix.

the overcoating. A listing of resins under consideration and their flow and cure properties is given in Table 12. Testing successfully demonstrated that the laboratory-scale overcoater at Vector Corporation could successfully overcoat approximately 2.5 kg of proppant in 45 min with an additional 15 min of drying time. This demonstrates the potential for this equipment and technology for production-scale processing for AGR TRISO fuel particles.

When the new equipment was delivered to B&W, it was determined that a 2 kg charge of fuel particles could be overcoated using a relatively low coating rate with exceptional accuracy and repeatability, even for making very high packing fraction compacts. Overcoating of NUCO fuel particles has provided the desired overcoating mass within 0.13% of the target to make 3440 g of overcoated particles/run (100% first pass yield). The overcoated particles had an aspect ratio of 1.018, an average particle size of approximately 1225 μm , and a particle size standard deviation of 46 μm . The NUCO prior to overcoating had an aspect ratio of 1.046, an average particle size of 847 μm , and a particle size standard deviation of 37 μm .

Initial compacting was done at ORNL, and a simple laboratory-scale compacting operation was set up at B&W's Lynchburg Technology Center. The operations comprised single-acting pistons

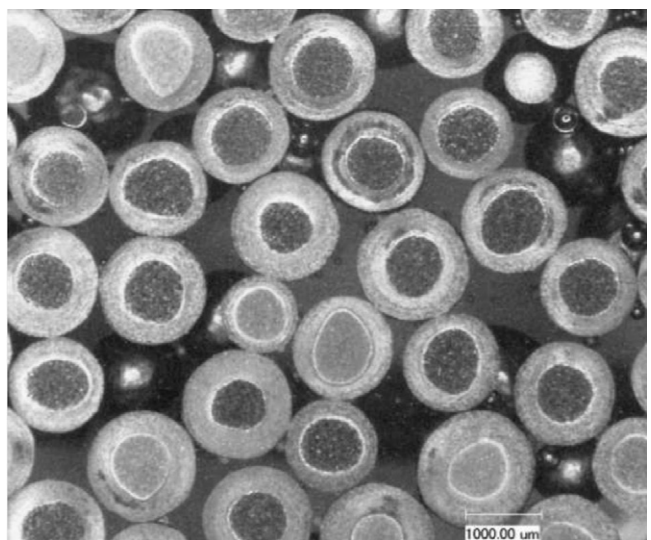


Fig. 22. Photomicrograph of overcoated surrogate proppant in cross section.

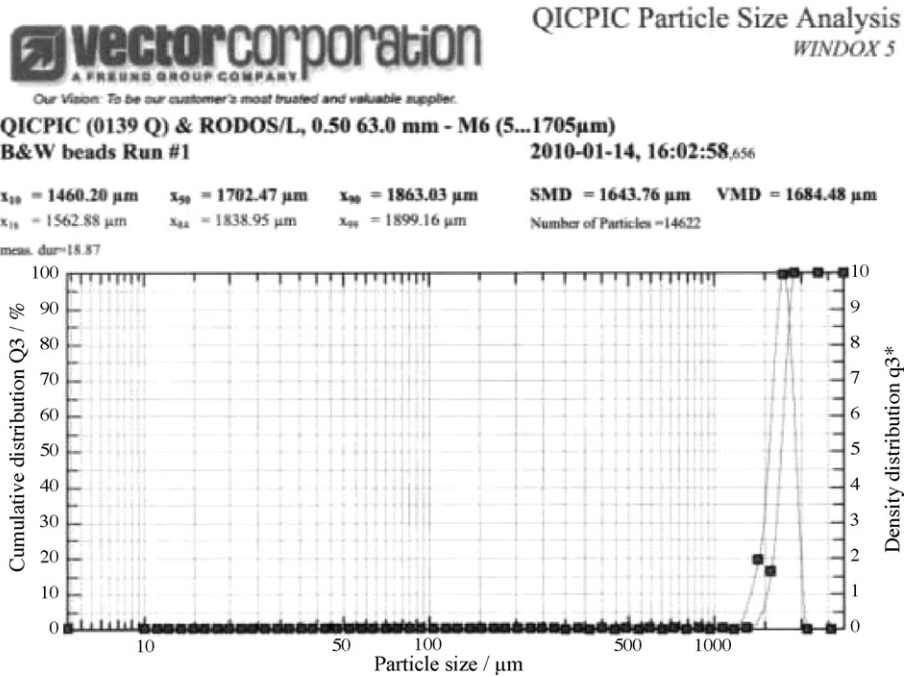


Fig. 23. Particle size analysis results on Vector overcoated proppant using QICPIC particle size analyzer.

Table 12

Hot press resins being considered and some key properties for each.

Resin	Type	Mettler drop point (°C)	Flow (mm)	Set time at 150 °C (s)	Comments
Plenco 14043	Standard Novolac + Hexa	100	45	70	Min. viscosity at 130 °C. Initial resin for overcoating tests and compacted to 1.73 g/cm ³ at 6.9 MPa
Hexion AD5614	Standard Novolac + Hexa	115	35	70	Min. viscosity at 130 °C. Used for second overcoating tests and compacted to 1.56 g/cm ³ at 6.9 MPa
Hexion D.SD-1708	High-purity Novolac	110	45	70 ^a	Direct replacement for Hexion AD5614
Hexion D.SD-1731	High-purity Novolac	110	110	70 ^a	Long flow version of SD-1708

^a When used with 8–10% Hexa cross linking agent.

mounted into a load frame, a compacting die, with heaters and controllers to regulate the die temperature. Compact charges, previously weighed out, were hand loaded into the die set, the hydraulic pump was actuated, and the load applied to the compact was monitored via a pressure gauge hooked into the hydraulic line. During compaction, the matrix melts and begins to flow under the compaction temperature in the die cavity, as shown in Fig. 24, to achieve initial die fill. Force is then held to increase the green density, and the matrix cures partially or fully in the die, depending on the temperature and time in the die. This provides for sufficient green strength to handle the compacts after hot pressing. Three compacts each were pressed under conditions listed in Table 13. Multiple matrix compositions were tested in this manner. After compacting for the desired time and load, the pressure was released, and the compact was ejected. The die temperature was regulated with a temperature controller and band heaters wrapped around the die set. Temperature stability during compacting was typically within ± 2 °C of the desired set point. After cooling, the ejected compacts were dimensionally inspected for height and diameter and then weighed.

After forming, the compacts were placed in a molybdenum boat. The furnace was evacuated to approximately 1.33 mPa and then purged with high-purity nitrogen gas at a flow rate of $\sim 67 \text{ cm}^3$ per second, which continued during the carbonization run. The chamber pressure under these conditions was approximately 13.30 kPa. The furnace was then ramped to the carbonization temperature of 800 °C and held for 1 h, followed by furnace cooling to room temperature. Initially, because of controller limitations, the furnace

temperature ramp rate was set at 4 °C/min versus the desired ramp rate of 2 °C/min. The compacts carbonized with this process exhibited no deleterious effects from this higher ramp rate, indicating that acceptable results can be obtained using a higher ramp rate

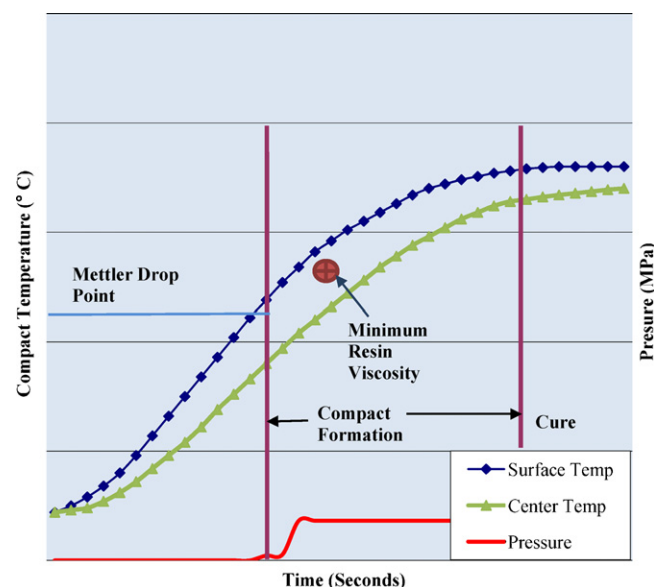


Fig. 24. Mettler drop point of Novolac resins and expected hot compaction schedule.

Table 13

Original compaction test matrix.

Sample	Die (°C)	Rate (MPa/sec)	Maximum pressure (MPa)	Time at load (sec)	Time to eject (sec)
Input parameters					
1	120	0.7	3.66	240	255
2	120	0.7	3.66	240	255
3	120	1.8	3.66	240	252
4	120	1.5	7.33	240	250
5	120	1.5	7.33	240	255
6	120	3.7	7.33	240	252
7	130	0.7	3.66	120	130
8	130	0.7	3.66	120	135
9	130	1.8	3.66	120	132
10	130	1.5	7.33	120	130
11	130	1.5	7.33	120	135
12	130	3.7	7.33	120	132
13	135	1.8	3.66	90	95
14	135	1.8	7.33	90	97
15	135	3.7	7.33	90	100
16	140	1.8	3.66	60	65
17	140	1.8	7.33	60	67
18	140	3.7	7.33	60	65

and shorter carbonization cycle under partial vacuum. The compact density results indicated that higher compaction pressures (greater than 7.3 MPa) are necessary to achieve the target objective of 1.75 g/cm³ matrix density in the pressed and heat-treated compacts.

Photographs of carbonized compacts using the Hexion AD-5614 and Plenco 14043 resins are shown in Figs. 25 and 26, respectively. Both resins produced consistent compacts, indicating that the Hexion and Plenco resins are usable for this application under the parameters tested in this study.

Photomicrographs of the as-compacted matrix and proppant are shown in Figs. 27–29.

Fig. 27 shows evidence of unmilled graphite contamination from the testing with Hexion resin. This larger graphite was not present in trials with the Plenco resin and was not detected during particle-size analysis, leading researchers to conclude that the

Coupon: W001A

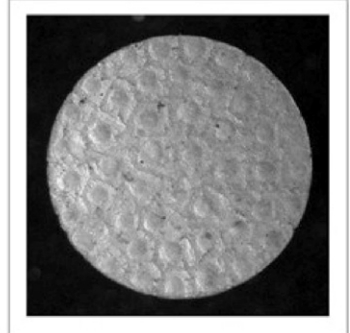
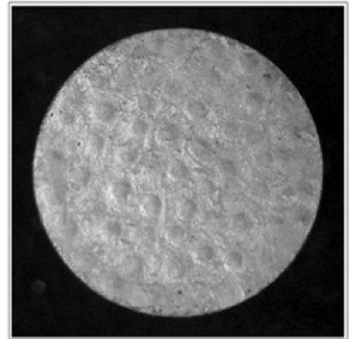
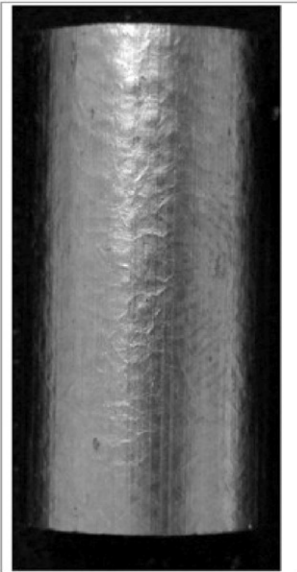


Fig. 26. Photograph of post-carbonization compact made at B&W from Plenco 14043 resin that was compacted at 120 °C and 7.33 MPa.

contamination was inadvertently introduced after jet milling of the materials. Evidence of matrix flow during compaction can be seen in Figs. 28 and 29. The Plenco resin was noted to have improved morphology and less segregation between the graphite and the resin compared to the Hexion AD-5614 resin. This can be seen in Fig. 29, where there are regions more rich in resin (darker regions) and regions more rich in graphite (lighter regions) that were not observed with the Plenco resin.

Additional compaction studies were performed using Plenco 14043 resin, Plenco 14433 resin, and Hexion SD-1708 resin with 7.5% Hexa. For these tests, spherical aluminum oxide media

Coupon: C006A

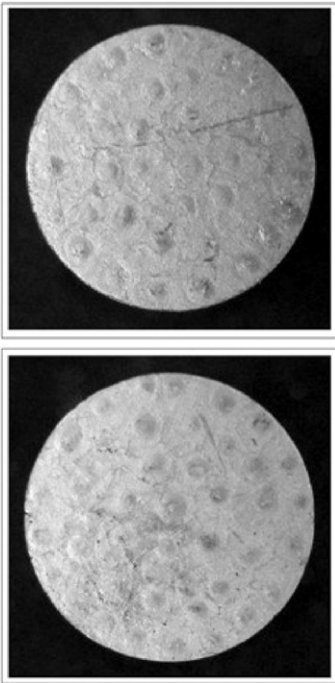
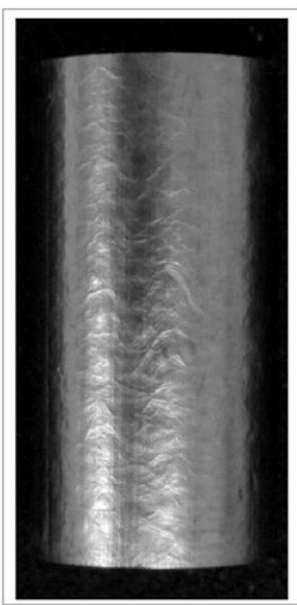


Fig. 25. Photograph of post-carbonization compact made at B&W from Hexion AD-5614 resin that was compacted at 120 °C and 7.33 MPa.

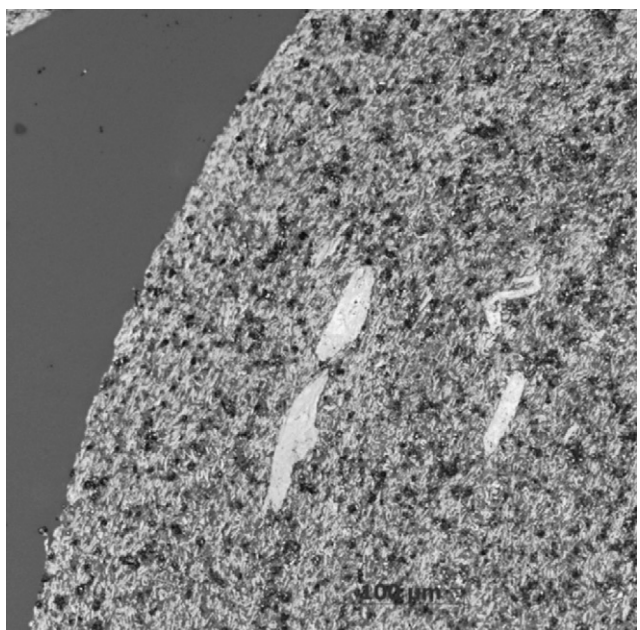


Fig. 27. Photomicrograph showing graphite in a parallel structure on particles, along with some unmilled graphite contamination in the matrix.

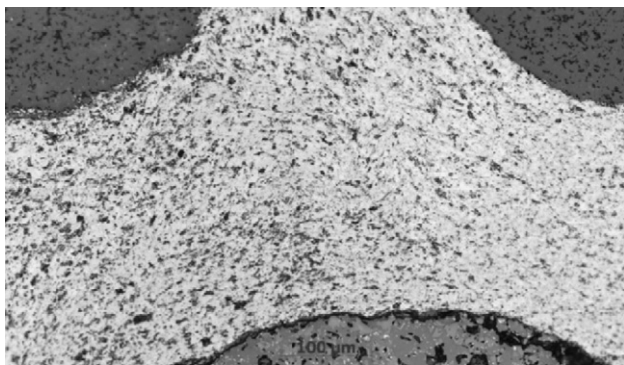


Fig. 28. Photomicrograph from the Plenco 14043 resin showing evidence of good flow during compaction.

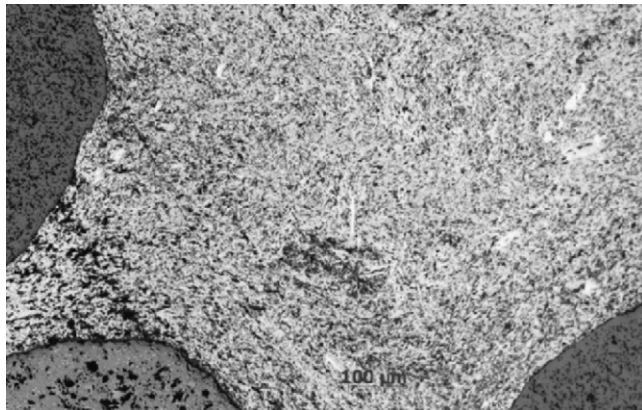


Fig. 29. Photomicrograph from the Hexion AD 5614 resin showing some evidence of segregation between the graphite and the resin.

were obtained from CoorsTek in a $-16/+18$ mesh size fraction (1000–1190 μm). A photograph of this material is shown in Fig. 30. This material was overcoated at Vector Corporation with the jet-milled matrix containing natural graphite, synthetic graphite, and the individual resin (Fig. 31). Examples of compacts made with each resin are shown in Figs. 32–34. Compacts were made from each resin during press acceptance testing at Miller Tool and Die Co., Jackson, MI. The results obtained with the most recent materials indicate that high matrix densities in excess of 1.75 g/cm^3 can be achieved using the Novolac resin matrix compositions.

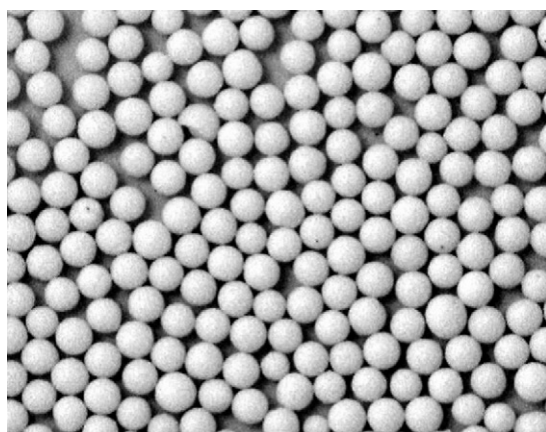


Fig. 30. Photograph of CoorsTek mini media with volume average particle size of 1180 μm used in earlier Vector overcoating trials.

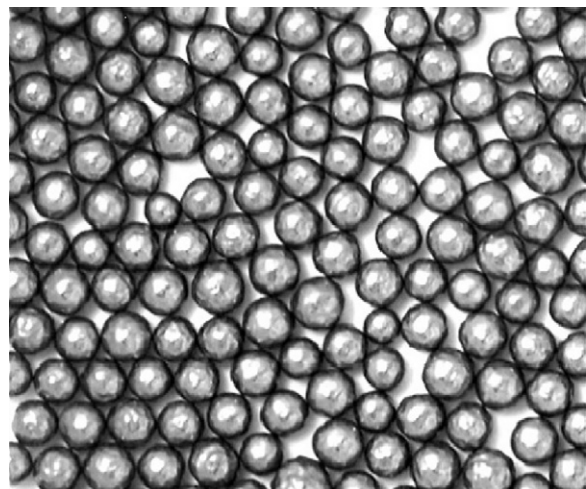


Fig. 31. Photograph of CoorsTek mini media overcoated using matrix with Hexion SD-1708 resin. The average particle size of the overcoated material is 1922 μm .

After installation of the overcoating, compacting, and heat-treatment equipment at B&W, shakedown tests were conducted. Initial testing used the Hexion SD-1708 resin with 7.5% Hexa added separately during milling. Overcoated particles and compacts were made on the new equipment using zirbead surrogate fuel particles for a 35% packing fraction using a 165 °C tooling preheat temperature and a 90-second pressing cycle at 18.1 MPa punch pressure. Seventy-two compacts made with these settings were characterized and heat treated. The compacts were shown to have a calculated matrix density of 1.765, and no cracking was observed as a result of heat treatment.

A process finalization testing sequence has now begun at B&W using NUCO fuel particles that allow use of fully prototypic processing conditions. Process tests are being performed at higher packing fractions and a range of temperatures, pressures, and hold times

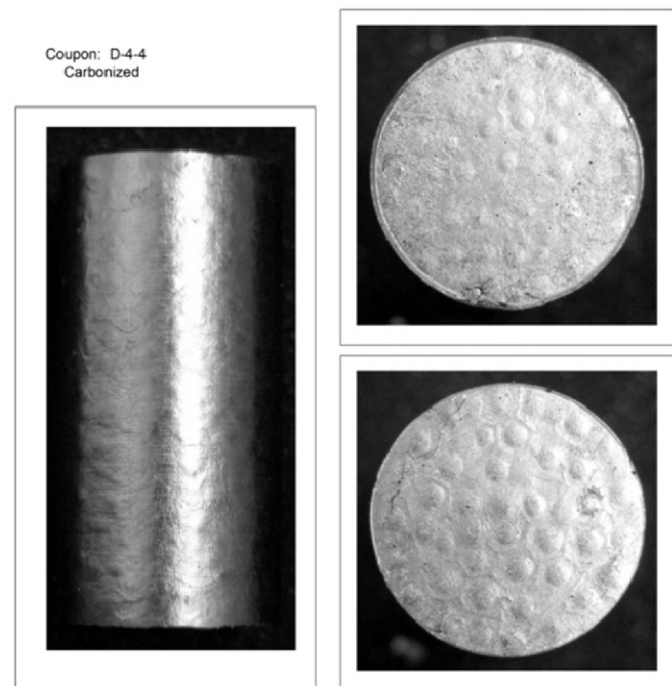


Fig. 32. Photograph of post-carbonization compact fabricated using Plenco 14043 resin pressed during press acceptance testing at Miller Tool and Die Co. at $\sim 18 \text{ MPa}$ and 130 °C with a 168 s hold time at pressure.

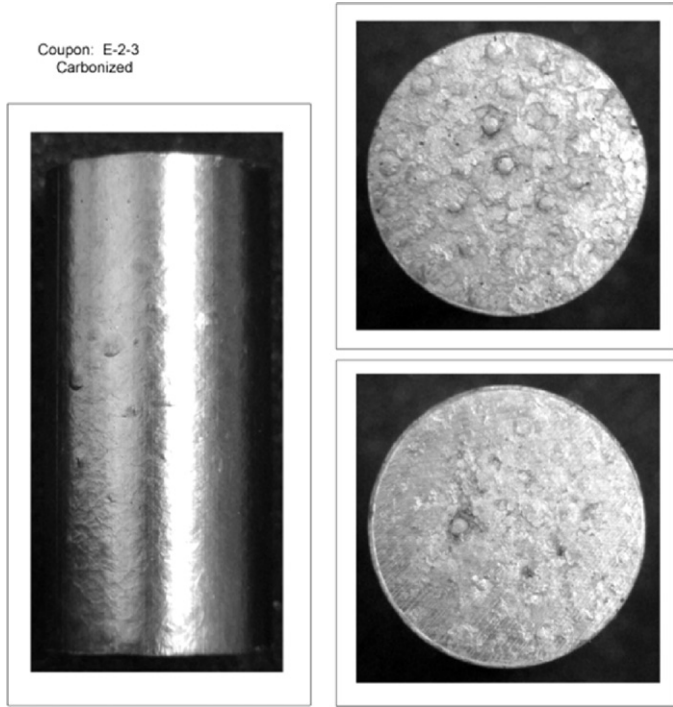


Fig. 33. Photograph of post-carbonization compact fabricated using Plenco 14433 resin pressed during press acceptance testing at Miller Tool and Die Co. at $\sim 11 \text{ MPa}$ and 130°C with a 168 s hold time at pressure.

to finalize process conditions for a minimum of two matrix compositions and two packing fractions. Process finalization will lead to certification of the line for use in fabrication of qualification test fuel to be made in 2012.

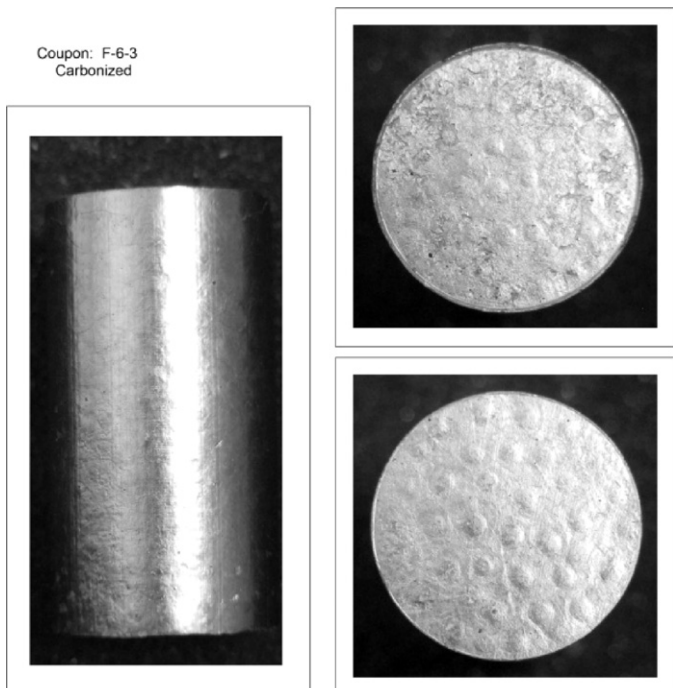


Fig. 34. Photograph of post-carbonization compact fabricated using Hexion SD-1708 resin pressed during press acceptance testing at Miller Tool and Die Co. at $\sim 11 \text{ MPa}$ and 150°C with a 90 s hold time at pressure.

15. Conclusions

Capability to fabricate high-quality UCO and UO_2 kernels for HTGR fuel has been established at B&W. The fabrication line has demonstrated production of 350- and 425- μm UCO kernels and 500- μm UO_2 kernels. High quality and high yields have been consistently achieved.

Several changes have also been successfully demonstrated that increase the process throughput or reduce run time. Additional steps are underway or planned for further increases in throughput of several unit operations. These include modifications to the wash/dry system to double the capacity of the kernel forming line, modifications to the acid deficient uranyl nitrate systems to reduce the cycle time, and increasing throughput of kernel upgrading.

Properties of AGR-2 fuel compare favorably with AGR-1 and historic German fuel. Kernels are more homogeneous in shape, chemistry, and density. TRISO-particle sphericity, layer thickness standard deviations, and defect fractions are also comparable. In a sample of 317,000 particles from deconsolidated AGR-2 compacts, 3 exposed kernels were found in a nitric acid leach test. No SiC defects in a sample of 250,000 deconsolidated particles and no IPyC defects in a sample of 64,000 particles were found. The primary difference in properties between AGR-1 and AGR-2 compacts is that AGR-2 compacts have a higher matrix density, 1.6 g/cm^3 compared to about 1.3 g/cm^3 for AGR-1 compacts. Based on fuel properties, excellent performance is expected for the AGR-2 UCO fuel.

Improvements were made to the kernel fabrication process to produce kernels with more homogeneous properties. Compared to historical HTR fuels, AGR kernels are more spherical and have a tighter distribution of aspect ratios.

The step change from coating in the 2-inch furnace used to produce AGR-1 particles to a 6-inch furnace used for AGR-2 particles was successful, and further improvement is expected. Defect fractions of AGR-2 particles were close to levels of the best German particles and within the range of other international TRISO-coated fuels. Additional coating development is continuing to maximize the charge size of the 6-inch furnace and consistently achieve low particle-defect fractions.

The success fabricating AGR-1 and AGR-2 fuels provides confidence that requirements for other AGR fuels can be met and the goals of the AGR program relative to reducing risks of HTR fuel fabrication can be accomplished.

The fluid-bed overcoating and hot-press compacting process approach selected for AGR compact scale-up is expected to provide significant improvements as a production method for compact fabrication through process simplicity and the application of new, improved technologies. Low unit-process reject rates and reduced or eliminated in-process particle upgrading and QC requirements are expected to boost first-pass yields above 95%.

The costs associated with fuel manufacturing are anticipated to decrease with respect to the current standard. The new methods are expected to provide faster turnaround and fewer processing steps. Process parameters are now being finalized at B&W using new process equipment and more definitive cost data to compare against other existing processes will be available within the next year.

Although the high-resin flow during hot-press compacting allows compact formation with higher matrix densities at low pressures, further adjustment of matrix preparation techniques may be needed to further homogenize the resin and graphite to minimize surface texture.

The scale-up team has successfully demonstrated the feasibility of overcoating TRISO particles using graphite (synthetic and natural) and phenolic resin with the matrix being applied using the Vector overcoating methodology. Batch sizes of up to 2.5 kg of

material can be overcoated without rejects in about an hour using this technique.

Trials on surrogate proppant resulted in an overcoated particle with sufficient green strength to allow for handling and transport of the overcoated material across the United States without damaging the overcoat. This material compacts reasonably well at relatively low compaction pressures (~3.7–7.3 MPa on a 1.24 cm diameter compact). Compacts made using these materials have strengths greater than AGR-2 compacts and are anticipated to prevent chipping or compact damage associated with handling.

In the original compaction trials, Plenco resin has provided a more homogenous morphology with better dispersion in the graphite matrix compared to the Hexion AD-5614 resin.

Follow up testing with the Hexion SD-1708 and Plenco 14043 resin with 7.5% Hexa provided an improved surface texture on coated particles, and particles created by both methods were less prone to cracking. Matrix-only compacts made from these resins exceeded 1.70 g/cm³ matrix density under normal hot-pressing conditions.

Initial shakedown testing with SD-1708 resin matrix at 7.5% Hexa resulted in compacts that would meet all design criteria, including matrix density. Process finalization testing is now in progress using NUCO fuel particles to evaluate the equipment and process performance using adjusted resin formulations at higher packing fractions and a variety of temperature-pressure-time relationships. Results from this phase of testing with NUCO are expected by October 2011.

Acknowledgments

This work was supported by the U.S. Department of Energy, Office of Nuclear Energy, under DOE Idaho Operations Office Contract DE-AC07-05ID14517. The authors wish to acknowledge the following individuals who contributed to this research and report: DeWayne L. Husser, Melvin L. Nowlin, and W. Clay Richardson from Babcock and Wilcox Nuclear Operations Group, Lynchburg, VA; and John D. Hunn from Oak Ridge National Laboratory, Oak Ridge, TN. The authors would also like to acknowledge the B&W operators whose work has contributed to the success of the AGR fuel fabrication program.

References

- Barnes, C.M., et al., 2008, September 28–October 1. Fabrication process and product quality improvements in advanced gas reactor UCO kernels. In: HTR2008-58039, 4th International Topical Meeting on High Temperature Reactor Technology, Washington, DC.
- Barnes, C.M., et al., 2009. Results of Tests to Demonstrate a Six-Inch Diameter Coater for Production of TRISO-Coated Particles for Advanced Gas Reactor Experiments. Paper HTR2008-58074. In: Proceedings of the 4th International Topical Meeting on High Temperature Reactor Technology, Washington, D.C., USA, September 28–October 1.
- Barnes, C.M., et al., 2010, October 18. Fabrication of uranium oxycarbide fuels for HTR fuel. Paper HTR2010-227, HTR-2010. In: Proceedings of the 5th International Topical Meeting on High Temperature Reactor Technology, Prague, Czech Republic.
- Beatty, R.L., Norman, R.E., Notz, K.J., 1979. Gel-Spere-Pac Fuel for thermal reactor – Assessment of fabrication technology and irradiation performance. ORNL/TM-5469.
- Bullock, R.E., 1993. Historical Review of Coated-Particle Fuel as Related to Performance of TRISO-P Particles. CEGA Interoffice Correspondence, CEGA-M-93-1274.
- Bullock, R.E., Sterling, S.A., 1977. Irradiation performance of HTGR fuel rods with diluted thermosetting matrices. Nucl. Eng. Des. 44, 109–123.
- Charollais, F., et al., 2004, September 22–24. CEA and AREVA R&D on HTR fuel fabrication & presentation of the GAIA experimental manufacturing line , 2nd International Topical Meeting on High Temperature Reactor Technology, Beijing, China.
- Charollais, F., et al., 2008. Latest achievements of CEA and AREVA NP on HTR fuel fabrication. Nucl. Eng. Des. 238, 2854–2860.
- Fu, X., et al., 2004. Preparation of UO₂ kernel for HTR-10 fuel element. J. Nucl. Sci. Technol. 41, 943–948.
- General Atomics, 1991. QC Data Package, NPR-MHTGR Performance Test Fuel, Test Capsules NPR-1, -1a, and -2, Coated Particles – Composite FM19-00001.
- Grover, B., et al., 2010, October 18. Completion of the first NGNP advanced gas reactor fuel irradiation experiment, AGR-1, in the advanced test reactor , Paper HTR2010-227, HTR-2010, Proceedings of the 5th International Topical Meeting on High Temperature Reactor Technology, Prague, Czech Republic.
- Hunn, J., 2004. Results from ORNL characterization of German reference fuel from EUO 2358–2365 composite. ORNL/CF-04/06.
- Hunt, R.D., et al., 2007. Preparation of spherical, dense uranium fuel kernels with carbon. Radiochim. Acta 95, 225–232.
- International Atomic Energy Agency, 1997. Fuel Performance and Fission Product Behavior in Gas Cooled Reactors. IAEA-TECDOC-978.
- Jellison Jr., G.E., Hunn, J.D., 2008. Optical anisotropy measurements of TRISO nuclear fuel particle cross-sections: the method. J. Nucl. Mater. 372, 36–44.
- Jellison Jr., G.E., et al., 2006. Optical characterization of tristructural isotropic fuel particle cross-sections using generalized ellipsometry. J. Nucl. Mater. 352, 6–12.
- Kasten, P., 1981. Comparative Evaluation of Pebble-Bed and Prismatic Fueled High-Temperature Gas-Cooled Reactors, Oak Ridge National Laboratory Report ORNL-5694.
- Keeley, J.T., Tomlin, B.L., 2008, September 28–October 1. Development of a continuous CVD process for TRISO coating of AGR fuel. Paper HTR2008-58008 , Proceedings of the 4th International Topical Meeting on High Temperature Reactor Technology, Washington, DC.
- Lowden, R.A., 2006. Fabrication of Baseline and Variant Particle Fuel for AGR-1. ORNL/CF-06/02, Rev. 0.
- Mehner, W., et al., 1990. Spacial fuel elements for advanced HTR manufacture and qualification by irradiation testing. J. Nucl. Mater. 171, 9–18.
- Minato, K., et al., 1994. Internal flaws in the silicon carbide coating of fuel particles for high-temperature gas-cooled reactors. Nucl. Technol. 106, 342–349.
- Morris, R.N., et al., 2004. TRISO-Coated Particle Fuel Phenomenon Identification and Ranking Tables (PIRTs) for Fission Product Transport Due to Manufacturing, Operations, and Accidents: Main Report. NUREG/CR-6844, Vol. 1.
- Nabielek, H., et al., 2004. Can we predict coated particle failure? A conversation on CONVOL, PANAMA and other codes , Technical Meeting on Current Status and Future Prospects of Gas Cooled Reactor Fuels, IAEA, Vienna, Austria, June 7–9.
- National Electrical Safety CodeC2-, 2007. The Institute of Electrical and Electronic Engineers, Inc.
- Pappano, P., 2007. Summary Report for the Initiation of Compact Development for Particles with 425-micron Kernels, Oak Ridge National Laboratory Report ORNL/TM-2007/161.
- Petti, D.A., Bell, G., 2005, May 15–19. The DOE Advanced Gas Reactor (AGR) Fuel Development and Qualification Program. In: International Congress on Advances in Nuclear Power Plants.
- Petti, D.A., et al., 2002. Key Differences in the Fabrication, Irradiation and Safety Testing of U.S. and German TRISO-coated Particle Fuel and Their Implications on Fuel Performance. INEEL/EXT-02-0300.
- Petti, D., Hobbins, R., Kendall, J., 2008. Technical Program Plan for the Next Generation Nuclear Plant/Advanced Gas Reactor Fuel Development and Qualification Program. INL/ECT-05-00465, Rev. 2.
- Sawa, K., Minato, K., 1999. An investigation of irradiation performance of high burn-up HTGR fuel. J. Nucl. Sci. Technol. 36, 781–791.
- Scott, C. S., Kovacs, W. J., 1977. General Atomics internal memo CSJ:007:FMB:77, September 1977. SiC Flaws Revisited – Part II, Correlation with Irradiation Performance.
- Vaidya, V.N., 2008. Status of sol–gel process for nuclear fuels. J. Sol–Gel Technol. 46, 369–381.
- Venter, J.H., Nabielek, H., 2006, October 1–4. Fuel: performance envelope of modern HTR TRISO fuel report. Paper H0000080 , 3rd Int. Topical Meeting on High Temperature Reactor Technology, Johannesburg, South Africa.